



Design and synthesis of a new bifunctional chelating agent: Application for Al ¹⁸F/¹⁷⁷Lu complexation

Wagner Laurène^{a,b}, Losantos Raúl^{c,d}, Selmeczi Katalin^e, Frochot Céline^f, Karcher Gilles^b, Monari Antonio^c, Collet Charlotte^{b,g,*}, Acherar Samir^{a,**}

^a Université de Lorraine, CNRS, LCPM, F-54000 Nancy, France

^b Nancyclotep, Plateforme d'imagerie moléculaire, F-54511 Vandœuvre-lès-Nancy, France

^c Université Paris Cité, CNRS, ITODYS, F-75006 Paris, France

^d Department of Chemistry, CISQ, Universidad de La Rioja, 26004 Logroño, Spain

^e Université de Lorraine, CNRS, L2CM, F-54000 Nancy, France

^f Université de Lorraine, CNRS, LRGP, F-54000 Nancy, France

^g Université de Lorraine, INSERM, IADI, F-54000 Nancy, France

ARTICLE INFO

Keywords:

Chelating agent
Radiolabeling
Aluminum-fluoride-18
Lutetium-177
Molecular modeling
Theranostic

ABSTRACT

Theranostic and personalized medicine are blooming strategies to improve oncologic patients' health care and facilitate early treatment. While ¹⁸F-radiochemistry for theranostic application is attractive due to its imaging properties, combining diagnosis by positron emission tomography (PET) via aluminum-fluoride-18 and β⁻ therapy with lutetium-177 is relevant. Nevertheless, it requires the use of two different chelating agents, which are NOTA and DOTA for aluminum-fluoride-18 and lutetium-177 radiolabeling, respectively. To overcome this issue, we propose herein the synthesis of a new hybrid chelating agent named **NO2A-AHM**, which can be labeled with different types of emitters (β⁺, β⁻ and γ) using the mismatched Al¹⁸F/¹⁷⁷Lu pair. **NO2A-AHM**, is based on a hydrazine moiety functionalized by a NOTA cycle, a chelating arm, and a linker with a maleimide function. This design is chosen to increase the flexibility and allow the formation of 5 up to 7 coordination bonds with metal ions. Moreover, this agent can be coupled to targeting moieties containing a thiol function, such as peptides, to increase selectivity towards specific cancer cells. Experimental complexation and computational chemistry studies are performed to confirm the capacity of our chelating agent to label both aluminum-fluoride and lutetium using molecular modeling approaches at Density Functional Theory (DFT) level.

The proof of concept of the ability of **NO2A-AHM** to complex both aluminum-fluoride-18, for PET imaging applications, and lutetium-177 for radiotherapy has shown encouraging results which is prominent for the development of a fully consistent theranostic approach.

Abbreviations: ACN, Acetonitrile; BFC, BiFunctional Chelator; Boc, tert-butoxycarbonyl; COSY, COrrrelation Spectroscopy; dc., Decay corrected; DCM, Dichloromethane; DFT, Density Functional Theory; DIEA, *N,N*-diisopropylethylamine; DMF, *N,N*-Dimethylformamide; DMSO, Dimethylsulfoxide; DOTA, 1,4,7,10-tetraazacyclododecane-1,4,7,10-tetraacetic acid; DOTATATE, DOTA-tyrosine-3-octreotate; DTPA, Diethylenetriaminepentaacetic acid; DUPA, 3-(1,3-dicarboxypropyl)-ureido]pentanedioic acid; equiv., Equivalent; ESI, ElectroSpray Ionization; EtOH, Ethanol; fr, Frontal report; HATU, 1-[Bis(dimethylamino)methylene]-1H-1,2,3-triazolo[4,5-b]pyridinium 3-oxid hexafluorophosphate; HBED, *N,N'*-Bis(2-hydroxybenzyl) ethylenediamine-*N,N'*-diacetic acid; HMBC, Heteronuclear Multiple Bond Correlation; HSQC, Heteronuclear Single Quantum Coherence; RP-HPLC, Reverse Phase High Performance Liquid Chromatography; LC-MS, Liquid Chromatography - Mass Spectrometry; MS, Mass Spectrometry; NETA, {4-[2-(bis-carboxymethylamino)-ethyl]7-carboxymethyl-[1,4,7]triazonan-1-yl}acetic acid; NMM, *N*-methylmorpholine; NMR, Magnetic Nuclear Resonance; NO2AtBu, Di-tert-butyl 2,2'-(1,4,7-triazonane-1,4-diyl)diacetate; NODAGA, 1,4,7-Triazacyclononane-1,4-glutaric acid-4,7-acetic acid; NODA, 1,4-Triazacyclononane-1,4-disacetic acid; NOTA, 1,4,7-Triazacyclononane-1,4,7-trisacetic acid; PET, Positron Emission Tomography; PSMA, Prostate Specific Membrane Antigen; RT, Room temperature; R_t, Retention time; S_N2, Nucleophilic substitution of type 2; SPECT, Single Photon Emission Computed Tomography; *t*Bu, tert-butyl; TFA, Trifluoroacetic acid; TLC, Thin Layer Chromatography; TRT, Targeted Radionuclide Therapy; UV, Ultra-violet.

* Corresponding author at: Nancyclotep, Plateforme d'imagerie moléculaire, F-54511 Vandœuvre-lès-Nancy, France.

** Corresponding author at: Université de Lorraine, CNRS, LCPM, F-54000 Nancy, France.

E-mail addresses: charlotte.collet@univ-lorraine.fr (C. Charlotte), samir.acherar@univ-lorraine.fr (A. Samir).

<https://doi.org/10.1016/j.jinorgbio.2023.112267>

Received 23 February 2023; Received in revised form 9 May 2023; Accepted 23 May 2023

Available online 2 June 2023

0162-0134/© 2023 Elsevier Inc. All rights reserved.

1. Introduction

The diagnosis and treatment of cancers through nuclear medicine have been improved during the last years due to the development of novel radiopharmaceutical targeting systems. Indeed, the discovery of cancer-type specific receptor on tumor cells allows the development of specific binding compound to target these receptors and hence the tumoral tissues. During the last four decades, the development of new radiopharmaceuticals with highly specific targeting capabilities has emerged in the field of nuclear medicine. These new radiopharmaceuticals allow patients health care improvement by offering more specific radiotracers for the precise diagnostic of numerous pathologies by nuclear imaging and their treatment by targeted radionuclide therapy (TRT). [1,2] These two diagnosis and treatment modalities are combined under the theranostic approach allowing access to personalized medicine. This approach consists in using the same radiopharmaceutical labeled either with a β^+ -emitter for positron emission tomography (PET) imaging or with γ -emitter for single photon emission computed tomography (SPECT) imaging for diagnosis or labeled with α - or β^- -emitters for treatment. A radiopharmaceutical is composed of a targeting entity coupled *via* a linker to a chelating agent which binds a radionuclide.

Radionuclides used in the theranostic approach are essentially radiometals requiring labeling *via* coordination bonds formation. The most common strategy up to date to ensure this aim is the labeling of the same compound with matched pairs of radionuclides for both diagnostic and therapy ($^{64}\text{Cu}/^{67}\text{Cu}$, [3] $^{44}\text{Sc}/^{47}\text{Sc}$, [4] $^{149}\text{Tb}/^{152}\text{Tb}/^{155}\text{Tb}/^{161}\text{Tb}$ [5]). [6] Nevertheless, a majority of these radioemitters are not yet used in clinical routine, hence seriously limiting this approach. An alternative strategy involves the use of mismatched pairs ($^{68}\text{Ga}/^{177}\text{Lu}$, [7] $^{44}\text{Sc}/^{177}\text{Lu}$, [8] $^{68}\text{Ga}/^{90}\text{Y}$, $^{64}\text{Cu}/^{90}\text{Y}$ [9]) with two different radionuclides to radiolabel the same compound.

The targeting agent is essential to provide adapted biological properties to the radiopharmaceutical (biodistribution, tumor uptake, dosimetry, clearance...). Numerous specific targeting agents are known

to bind selectively to receptors overexpressed on tumor cells and are essentially biomolecules like peptides, proteins, or antibodies. A significant number of radiopharmaceuticals employing the mismatched pairs $^{68}\text{Ga}/^{177}\text{Lu}$ showed excellent clinical success. The first one is the couple [^{68}Ga]Ga-DOTATATE/[^{177}Lu]Lu-DOTATATE (Luthatera®) targeting the somatostatin receptor, overexpressed on neuroendocrine tumors. These radiotracers are composed of the octreotide peptide as targeting agent, DOTA chelator as a bifunctional chelator (BFC), and gallium-68 for diagnosis or lutetium-177 for treatment. For prostate cancer, the prostate-specific membrane antigen (PSMA) receptor is targeted by the 2-[3-(1,3-dicarboxypropyl)-ureido]pentanedioic acid (DUPA) pattern and is contained in the radiopharmaceuticals [^{68}Ga]Ga-PSMA-11 and [^{177}Lu]Lu-PSMA-617 (Pluvicto®). [10] This strategy offers a similar biodistribution profile with the use of radionuclides commonly used for clinical applications ($^{68}\text{Ga}/^{177}\text{Lu}$).

Recent advances in fluoride-18 radiochemistry have been made in particular by the novel strategy developed by McBride et al. in 2009 allowing the direct labeling of fluoride-18 by complexation. The so-called “aluminum-fluoride-18” strategy consists in the complexation of an aluminum atom by a chelator and fluorine-18, this former playing the role of a co-ligand. [11] Furthermore, this innovative strategy opens the gate to new mismatched theranostic pairs such as $\text{Al}^{18}\text{F}/^{177}\text{Lu}$ in the development of new radiopharmaceuticals but the need of adapted BFC is crucial.

BFCs were developed to link the radionuclide to the targeting agent. The BFC is covalently coupled to the targeting agent and the radiometal is fixed to it through the formation of coordination bonds. Numerous BFCs have been developed (Fig. 1) including acyclic chelating agents such as diethylenetriaminepentaacetic acid (DTPA), *N,N'*-bis-[2-hydroxy-5-(carboxyethyl)benzyl]ethylenediamine-*N,N'*-diacetic acid (HBED-CC), or cyclic chelating agent like 1,4,7-triazacyclononane-1,4,7-triacetic acid (NOTA) and its derivatives 1,4,7-triazacyclononane,1-glutaric acid-4,7-acetic acid (NODAGA) and {4-[2-(bis-carboxymethylamino)-ethyl]7-carboxymethyl-[1,4,7]triazonan-1-yl}acetic acid (NETA), 1,4,7,10-tetraazacyclododecane-*N,N',N'',N'''*-tetraacetic

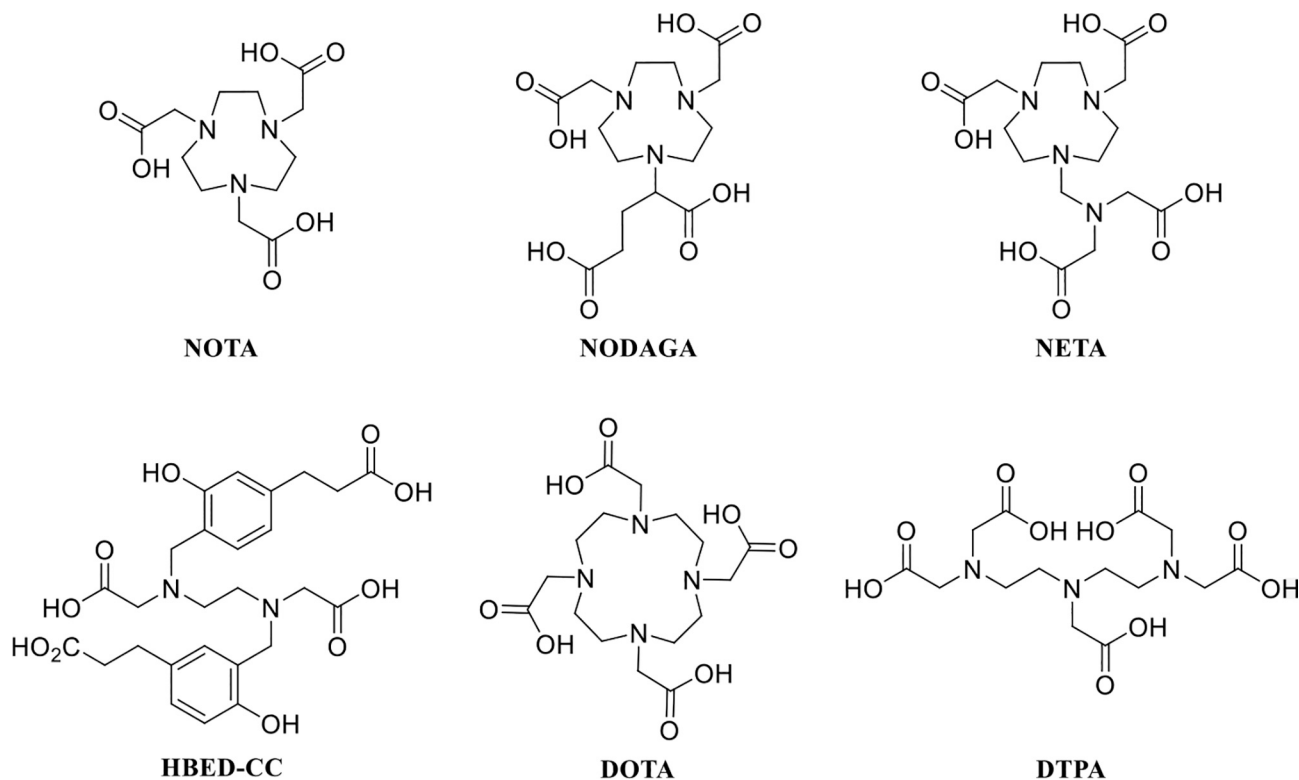


Fig. 1. Chemical structures of chelators used for Al^{18}F -labeling and for ^{177}Lu -labeling.

acid (DOTA) to complex diagnostic and therapeutic radionuclides. [12]

Nevertheless, the choice of the chelating agent depends on the radiometal to prevent the off-target side effect. Thus, using those chelators can limit the development of theranostic agents as one chelator cannot form stable complexes with all radiometals. Various coupling strategies have been studied to link the targeting agent to the BFC, among them the irreversible bioconjugation reaction with formation of an amide bond is well described. However, this strategy involves the use of preliminary protected chelators and targeting agents and is prone to degradation by proteases. Other bioconjugation strategies such as thiol-maleimide click reactions or the formation of thiourea thanks to isothiocyanate (NCS) function are also commonly used. These reactions are fast, complete in mild reaction conditions (physiological conditions, room temperature) and are selective towards thiol or amine functions respectively, thus enabling to carry out coupling reactions with unprotected targeting agents.

Fluoride-18 is the most used β^+ -emitter (half-life of 110 min, mean β^+ (95%) energy of 250 keV), is produced through a cyclotron ($^{18}\text{O}(p, n)^{18}\text{F}$) and provides PET images with high spatial resolution. Since it is a halogen atom, it must be coupled to the targeting agents *via* covalent bonding. The indirect substitution approach employing prosthetic groups is the most widespread strategy of radiofluorination, despite this strategy has limitation regarding the time of radiosynthesis and radiochemical yield. [13] The “aluminum-fluoride-18” strategy takes advantage of the easiness of the metal-ion chelating approach. Indeed, the $\{\text{Al}^{18}\text{F}\}^{2+}$ forms five coordination bonds with chelating agents with, for example, acyclic chelator HBED-CC and cyclic chelator based on NOTA cycles like NODAGA and NETA. This chelator size is the most adapted for $\{\text{Al}^{18}\text{F}\}^{2+}$ complexation providing high radiochemical incorporation yield. [14,15]

Lutetium-177 (half-life of 6.7 days) is an element belonging to the lanthanide group, often used for TRT due to its β^- -emission (β^- (100%), mean β^- energy of 134 keV) and its γ -radiation (γ , 113 keV (6.4%), 208 keV (11%)) allowing an efficient monitoring of treatment by SPECT imaging. Lu^{3+} ion can form from six to nine coordination bonds and can be complexed by cyclic chelators presenting a large cavity size (DOTA), besides of acyclic chelators (DTPA). [16] Some research groups have considered the chelation of lutetium-177 with a small cyclic cage like NOTA but decomplexation has been observed in some cases [17,18] albeit contrasting results are reported. [19] The poor stability of ^{177}Lu -NOTA complex could be principally due to the insufficient number of donor group (5–6) to fully saturate the coordination sphere of the metal ion (preferential coordination number between 8 and 9).

The development of theranostic agents using $\text{Al}^{18}\text{F}/^{177}\text{Lu}$ mismatched pair is less studied as none of commonly used chelators have the ability to complex both elements. Lepage et al. have been the first to investigate the development of a theranostic agent for the mismatch pair $^{18}\text{F}/^{177}\text{Lu}$. The radiotracer was developed with two label units, a DOTA cycle for lutetium-177 radiolabeling and an organotrifluoroborate prosthetic group for fluoride-18 radiolabeling providing the compound DOTA-AMBF3-PSMA for use in the treatment of prostate cancer by

means of nuclear medicine through theranostic approach. [20]

The first study on the development of BFCs for theranostic approach was conducted by Chong and coworkers. [21] BFCs were designed as derivatives from NETA chelator such as C-NE3TA [22,23] and 3p-C-NETA [24,25], representing hybrid cyclic/acyclic chelating agents combining a NETA macrocyclic ring with additional chelating arms and possessing an asymmetric carbon.

The 3p-C-NETA had shown its ability to be labeled by a large panel of radiometals (aluminum-fluoride-18, copper-67, yttrium-90, terbium-161, lutetium-177 and bismuth-212/213). This strategy relies on the combination of the flexibility provided by an acyclic chelating arm and the greater stability afforded by a cyclic chelating agent. Moreover, nuclides with a large atomic radius (*e.g.*, lutetium) are not well stabilized by small cyclic chelating agents like NOTA and are placed on the top of the cycle leading to a non-octahedral geometry. Thus, adding a chelating arm may stabilize the complex by surrounding the radionuclide on the opposite side of the cycle and presenting an additional donor group to increase the coordination number between the metal and the chelator. Ahenkorah et al. studied the stability of 3p-C-NETA-based radioconjugates. [26] The good stability of the ^{18}F]AlF-3p-C-NETATATE, and ^{177}Lu]Lu-3p-C-NETATATE was observed both in PBS and human serum during 2 h and 10 days, respectively. Regarding ^{68}Ga]Ga-3p-C-NETATATE, a good stability of the complex was observed in PBS after 2 h but 45% of decomplexation was observed after 2 h in human serum. This result gave encouraging results for the development of theranostic agents using the mismatched pair $\text{Al}^{18}\text{F}/^{177}\text{Lu}$ using the same compound to label.

Concerning the impact of the charge of the radiometal-chelator complex, it has been described that they have a major influence on the pharmacokinetic properties of labeled peptides. [27–29] Despite, Baun et al. has shown that the biodistribution was unmodified for NOTA and NODAGA ^{68}Ga -complexes which are differently charged. Similar results were also described by Guo et al. by comparing the two radiopharmaceuticals ^{18}F]AlF-NOTA-PRGD2 and ^{68}Ga]Ga-NOTA-PRGD2 given respectively neutral and positively charged radiotracers. [30,31]

We therefore propose a new BFC, **NO2A-AHM**, (Fig. 2) and evaluate its ability to complex the mismatched $\text{Al}^{18}\text{F}/^{177}\text{Lu}$ pair to provide new radiopharmaceuticals for theranostic approach. Our BFC is built around a hydrazine moiety which has the advantage to be easily functionalized by up to four groups thanks to its two nitrogen atoms, to be inert towards peptidases and to afford a good flexibility thanks to the sp^3 hybridization of the nitrogen atoms. Moreover, compounds having a hydrazine moiety have the advantage to present any asymmetric carbon. The originality is based on the use of the hydrazine moiety functionalized by a cyclic chelator (NOTA), and a chelating arm to elaborate a hybrid cyclic and acyclic chelating agent. Thereby, this new chelating agent could complex various radiometals with a NOTA cycle for small ionic radius elements (*i.e.*, aluminum) while being able to accommodate larger ionic radius elements thanks to additional chelating arm (*i.e.*, lutetium). Indeed, the number of donor groups would adapt in function of radionuclides, providing from five to seven coordination bonds, thus increasing the stability regarding its complex with NOTA alone. Thiol-maleimide click chemistry reaction was chosen to link the targeting agent, since it is fast and total in mild conditions while being selective to thiol function when using unprotected peptides. Thus, the hydrazine moiety is also functionalized by a linker presenting a terminal maleimide function to couple the BFC to a large panel of targeting agents with a thiol function, such as peptides or antibodies. The synthesis and characterization of this new BFC is described. Then molecular modeling investigation to study the atoms of the BFC involved in the complexation is performed, following by the complexation evaluation of the BFC with aluminum-fluoride and lutetium. To evaluate the perspective of application of this new BFC to be used for radiopharmaceutical purpose, preliminary radiolabeling tests were done.

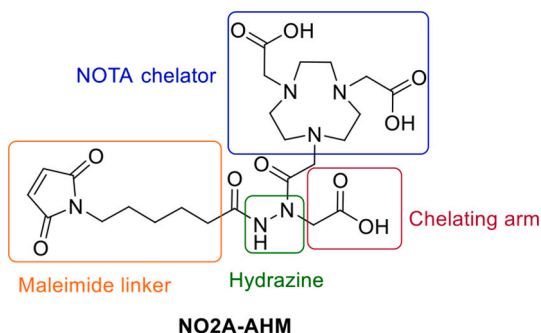


Fig. 2. Chemical structure of the new BFC NO2A-AHM.

2. Results and discussion

2.1. Synthesis of NO2A-AHM

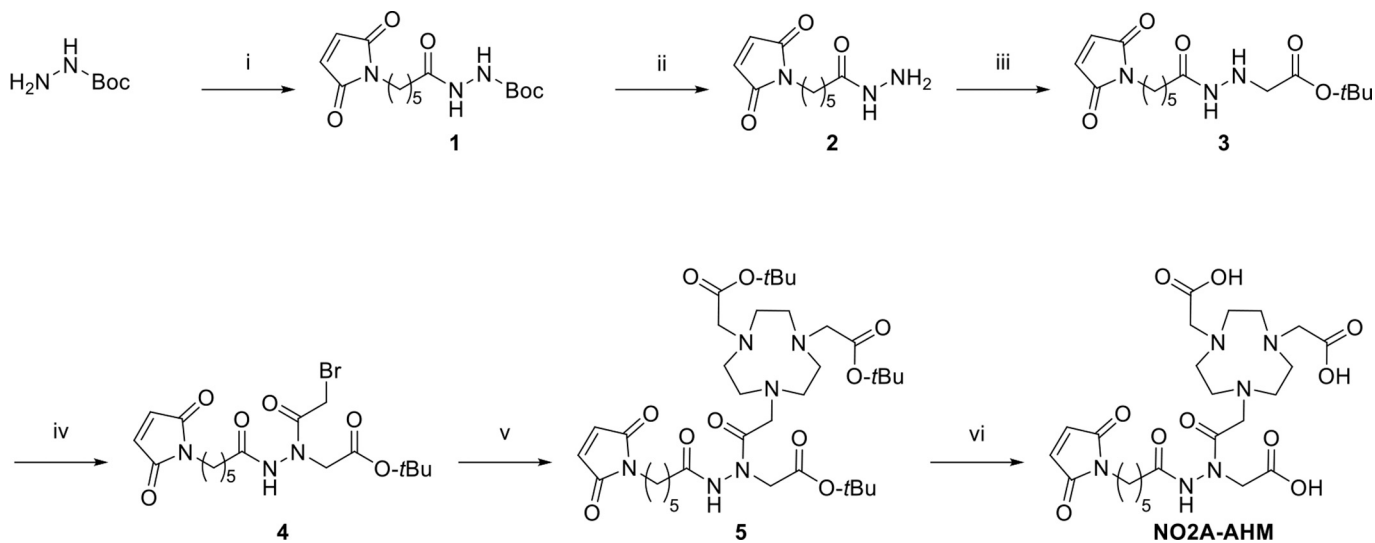
The synthetic strategy consisted in the functionalization of a hydrazine molecule with three entities (NOTA cycle, chelating arm and maleimide linker). The addition order of the three entities was determined to firstly introduce the maleimide linker, secondly the chelating arm and finally the NOTA cycle (Scheme 1).

Firstly, the coupling of the maleimide linker to the free amino group of the commercially available starting material *tert*-butyl carbamate by amidation was achieved under classical peptide coupling conditions (*i.e.*, HATU as activator, NMM, stirred in DMF for 5 h at room temperature (RT). [32,33] After purification on silica gel using DCM/EtOH (98/2, *v/v*), compound **1** was obtained with a high yield of 91% and a purity of 95% determined by HPLC at 214 nm (Step i, Scheme 1). Then, the Boc protecting group was removed with an excess of TFA in DCM at RT for 5 h. After precipitation in cooled Et₂O (−20 °C) and centrifugation, the compound **2** was afforded as a white solid with a purity of 95% at 214 nm and a quantitative yield (Step ii, Scheme 1).

The next step has consisted in the coupling of the chelating arm using a S_N2 reaction between the compound **2** and *tert*-butyl bromoacetate. This reaction has shown the formation of the willing compound **3** and the dialkylated compound **3'**. Results of the optimization allowing to increase the ratio mono-bialkylated **3/3'** products are described in Table SI-1. The use of DMF, 1.1 equiv. of K₂CO₃ and 1 equiv. of *tert*-butyl bromoacetate (Condition 8, Table SI-1) based on Lubell and coworkers' procedure, [34,35] has conducted to a **3/3'** ratio of 81/19 with only 4 ± 3% of remained compound **2**, thus providing an isolated yield of compound **3** of 53%. The next step was the addition of a bromoacetyl function on the hydrazine of compound **3** through an acylation reaction using bromoacetyl bromide [36] (Step iv, Scheme 1). This reaction produced HBr specie which decreased the pH of the reaction mixture. Thus, a base has to be introduced in the reaction mixture to maintain a neutral pH during the reaction and to avoid the deprotection of the *t*Bu group. K₂CO₃ was tested initially (2 equiv.) but it did not increase the pH above 2. As a result, partial deprotection of the *t*Bu group was observed 10 min after the addition of bromoacetyl bromide. We noted that the addition of an organic base like pyridine (1.5 equiv.) was efficient to stabilize the pH at a value of 7 and helped avoid the *t*Bu deprotection. The acylation reaction was completed in 15 min leading to the desired compound **4** in an excellent yield of 89% with a purity of 96%

determined by HPLC at 214 nm. The NOTA chelator was then coupled to compound **4** to afford compound **5** via an S_N2 reaction between the bromine atom on compound **4** and the secondary amine of commercially available NO₂AtBu under basic conditions to increase the nucleophilic characters of this secondary amine (Step v, Scheme 1) and neutralize HBr formed during the reaction. [37] The synthesis of compound **5** was performed by adding a solution of NO₂AtBu (0.9 equiv.) and a base in anhydrous ACN to a solution of compound **4** (1 equiv.) in anhydrous ACN at 0 °C and then stirred at RT for 20 h. Different bases were evaluated (*i.e.*, DIEA, pyridine, K₂CO₃, Et₃N and NMM from 1 to 3 equiv.) to minimize the formation of the side-product **5'** relative to the formation of the desired compound **5** (Table SI-2). This by-product **5'** resulted from the coupling of two NO₂AtBu cycles with the compound **4** via an S_N2 reaction of the bromine atom following by an aza-Michael addition reaction on the maleimide function. Aza-Michael additions of a wider range of amines (*e.g.*, primary, secondary, acyclic and cyclic) [38] and maleimides are known from the literature. Among others, it was shown that in simultaneous presence of thiol and primary amine groups, a competition between thiol- and aza-Michael additions occurred in aqueous buffer. [39] Chemoselective thiol-Michael additions were observed from pH 6.5 to 7.5, but above this pH range (up to pH 7.5), primary amines competed directly with the thiol groups in Michael additions (*i.e.*, loss of thiol chemoselectivity) due to the increasing nucleophilicity of the amines. These findings would tend to suggest that the pH during the reaction must be under 7.5 to disfavor the formation of the by-product **5'**, but at the same time, it should be high enough to allow S_N2 reaction. It would therefore seem that a neutral pH of 7.0 represents the optimal condition for minimizing by-product **5'** formation. The best result was achieved using a dropwise addition of the NO₂AtBu/DIEA (2 equiv.) solution for 2 h at 0 °C. This slow addition helped significantly to improve the **5/5'** ratio by up to 98/2 with a very high compound **4** consumption (*i.e.*, 2% remaining), resulting in an isolated compound **5** yield of 37%. Despite these optimized conditions, only 37% of compound **5** were isolated, and this was due to the difficulty in separating compound **5** from **5'** during the purification step.

Finally, *t*Bu protecting groups on compound **5** were removed with an excess of TFA in DCM (Step vi, Scheme 1). After precipitation in cooled Et₂O (−20 °C), centrifugation and purification by RP-C18 HPLC, the final compound **6** (*i.e.*, NO₂A-AHM) was afforded as a white solid with a purity of >98% at 214 nm and a quantitative yield (Step vi, Scheme 1). In summary, NO₂A-AHM was obtained in six steps with an overall yield of 16%. The two nucleophilic substitutions were the two limiting steps



Scheme 1. NO₂A-AHM synthesis. Reagents and conditions: (i) maleimido-hexanoic acid, HATU, NMM, DCM/DMF (1/1, *v/v*), RT, 5 h, 91%; (ii) TFA, DCM, RT, 5 h, quantitative; (iii) BrCH₂CO₂*t*Bu, K₂CO₃, DMF, RT, overnight, 53%; (iv) BrCH₂COBr, pyridine, DCM, RT, 20 min, 89%; (v) NO₂AtBu, DIEA, ACN, overnight, RT, 37%; (vi) TFA, DCM, RT, 5 h, quantitative.

(Steps iii and v, Scheme 1) with yields of 53% and 37%, respectively, after optimization of the reaction conditions.

2.2. Molecular modeling

Molecular modeling has been used to elucidate the main structural properties of the chosen ligands and complexes, and also due to the difficulties encountered in obtaining suitable crystals for structural analysis by X-Ray Diffraction. Firstly, aluminum complexes have been modeled demonstrating the ability of NO2A-AHM to complex the metal ion, different conformers varying on their coordination numbers have also been explored. Furthermore, the availability of coordination sites allowing the inclusion of fluoride has also been confirmed. The structures of the AlF-NO2A-AHM complex have been obtained as well and were systematically compared with those of Al/AlF to allow a direct comparison.

2.2.1. Optimized geometries

The coordination properties of NO2A-AHM towards aluminum mono-fluoride cation ($\{AlF\}^{2+}$) and lutetium cation (Lu^{3+}) were studied by molecular modeling under the framework of density functional theory (DFT). The optimized geometries for the most stable conformations and the calculated free energies determined for each complex are presented in Fig. 3.

2.2.1.1. Optimized geometry of AlF-NO2A-AHM. To fully evaluate the complexation between NO2A-AHM and trivalent aluminum (Al(III)), the stability of two different conformers were studied (Fig. 4). Thus, to explore the complex configurational space experienced by the chelating systems, we also modeled an additional hexacoordinated compound in which the oxygen of the amide function is directly coordinating aluminum (Hexa_Al_O=C). Interestingly, the latter appeared to be quasi-generated with Hexa_Al_arm, having a small free energy difference of 5.51 kcal.mol⁻¹. Consequently, and also depending on the energy barrier, both minima can be populated. Conversely, the saturation of the coordination sphere of Al with a fluoride resulted in the most favorable complex and yielded a remarkable stabilization compared to Hexa_Al_arm by 46.75 kcal.mol⁻¹.

Moreover, a comparison between the equilibrium geometries of Hexa_Al and Hexa_Al_F can be appreciated in Fig. 4. Both complexes were neutral and presented octahedral coordination around aluminum with a N₃O₂F first coordination sphere for Hexa_Al_F and N₃O₃ for Hexa_Al_arm. Aluminum was located at the center of the chelator ring and was coordinated by the three nitrogen atoms of the NOTA cycle, the two oxygen atoms of the carboxylate group of the alkyl side chains and the fluoride atom. The geometry was coherent with the DFT calculation reported by Wang et al. [40] Looking into more detailed geometrical parameters, the average Al–N and Al–O coordination distances were of 2.130 and 1.853 Å, respectively, and they behave similarly for the two complexes (Table SI-3). The relatively short bond lengths further corroborated the stability of the coordination between Al and the chelator. Indeed, even the presence of fluoride did not distort

significantly the coordination environment. However, the AlF bond in Hexa_Al_F, was significantly shorter (1.733 Å) than the other Al–N and Al–O bonds, as expected from the high affinity of fluoride for aluminum, as shown by its high stabilization energy estimated at around 580–670 kJ.mol⁻¹. [41] For both structures, a slightly distorted octahedron was observed as the 12 orthogonal and the 3 linear angles were close to the ideal values of 90° and 180°, respectively. The orthogonal angles were averaged at 89.809° for Hexa_Al_arm and 89.843° for Hexa_Al_F, while the linear angles were centered at 168.330° and 168.015°, respectively. Despite the high similarity between the two structures, the Hexa_Al_F geometry appeared slightly more distorted than Hexa_Al_arm. The average of the difference between the ideal orthogonal angles (90°) and the orthogonal angles was of 5.741° and 5.482°, respectively, and the average difference between the ideal linear angles (180°) and linear angles was of 11.984° and 11.670°, respectively. A similar distorted octahedral arrangement was observed in the X-ray structures of AlF-NODA presenting orthogonal and linear angles averaging at 89.89° and 169.60°, respectively. [41]

2.2.1.2. Optimized geometry of Lu-NO2A-AHM. The computational study was extended to Lu-NO2A-AHM complex. As lutetium is able to form complex with a chelator thanks to 6 to 9 coordination bonds, two hexacoordinated and one heptacoordinated conformations (Hexa_Lu_O=C, Hexa_Lu_arm and Hepta_Lu, respectively) were modeled to determine the most stable configuration. Also, the possible coordination of water was considered including 1, 2 or 3 molecules. The heptacoordinated structure was the most stable one compared to hexacoordinated and highly coordinative solvated species. The difference of energy between Hexa_Lu_O=C, Hexa_Lu_arm was significant (ΔG : 9.33 kcal.mol⁻¹) and demonstrated the importance of the chelating arm for the complexation of metal. Heptacoordinated complex had a similar energy compared to Hexa_Lu_arm (ΔG : 1.31 kcal.mol⁻¹) and hence should be populated at RT. All the solvated species were at least 5 kcal.mol⁻¹ above these two species, eventually discarding their formation in water environments.

Looking into the geometries of Hexa_Lu_arm and Hepta_Lu, some considerations concerning their structural parameters can be drawn, especially in comparison with the corresponding Al complexes. The hexacoordinated structure presented an octahedral geometry with lutetium as the center atom complexed by N₃O₃ donor set. The complexation sphere involved the three nitrogen atoms of the NOTA cycle, the two oxygen atoms of the carboxylate group of the alkyl side chains and the oxygen atom of the chelating arm (Table SI-4). The average Lu–N and Lu–O coordination bond lengths were of 2.527 and 2.148 Å, respectively, and hence longer than Al–N and Al–O coordination bond due to the larger atomic radius of lutetium (difference between Lu–N and Al–N bond length of 0.397 Å and difference between Lu–O and Al–O of 0.295 Å). These bond lengths demonstrated the strength of coordination of lutetium with the chelator. A distorted octahedron was observed as the 12 orthogonal and the 3 linear angles were close to the ideal values of 90° and 180°, respectively, the average of orthogonal angles being 89.476° and the average linear angles

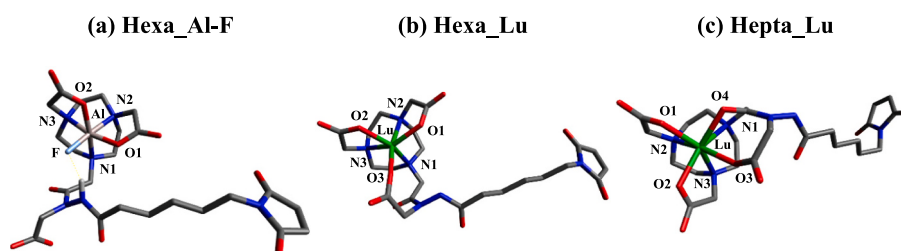


Fig. 3. Optimized geometries of AlF-NO2A-AHM (a) and Lu-NO2A-AHM (hexacoordinated (b) and heptacoordinated (c)). Hydrogens were removed for more clarity.

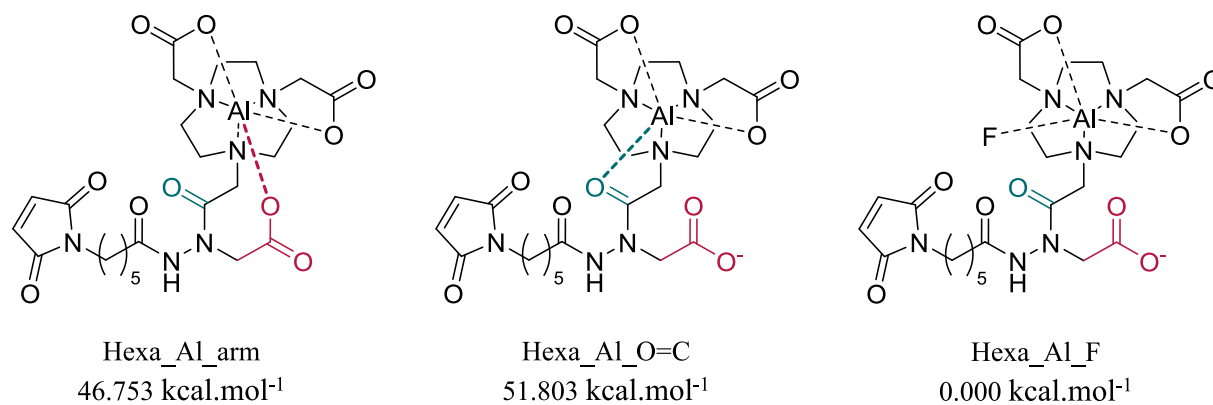


Fig. 4. Chemical structures of Al- and AlF-NO2A-AHM complexes studied in molecular modeling and their free energy (kcal.mol⁻¹) related to the free energy of Hexa_Al_F structure.

150.783°. The average of the difference between the ideal orthogonal angles (90°) and the orthogonal angles was of 15.318° and the average difference between the ideal linear angles (180°) and linear angles was of 29.217°. Thus, the Hexa_Lu geometry was more distorted than Hexa_Al_F geometry and this could be explained by a most important ring

deformation. The heptacoordinated structure presented distorted pentagonal bipyramidal geometries with lutetium as the center atom complexed by N₃O₄ donor set (complexation with the three nitrogen atoms of the NOTA cycle, the two oxygen atoms of the carboxylate group of the alkyl side chains, oxygen atom of the chelating arm and the

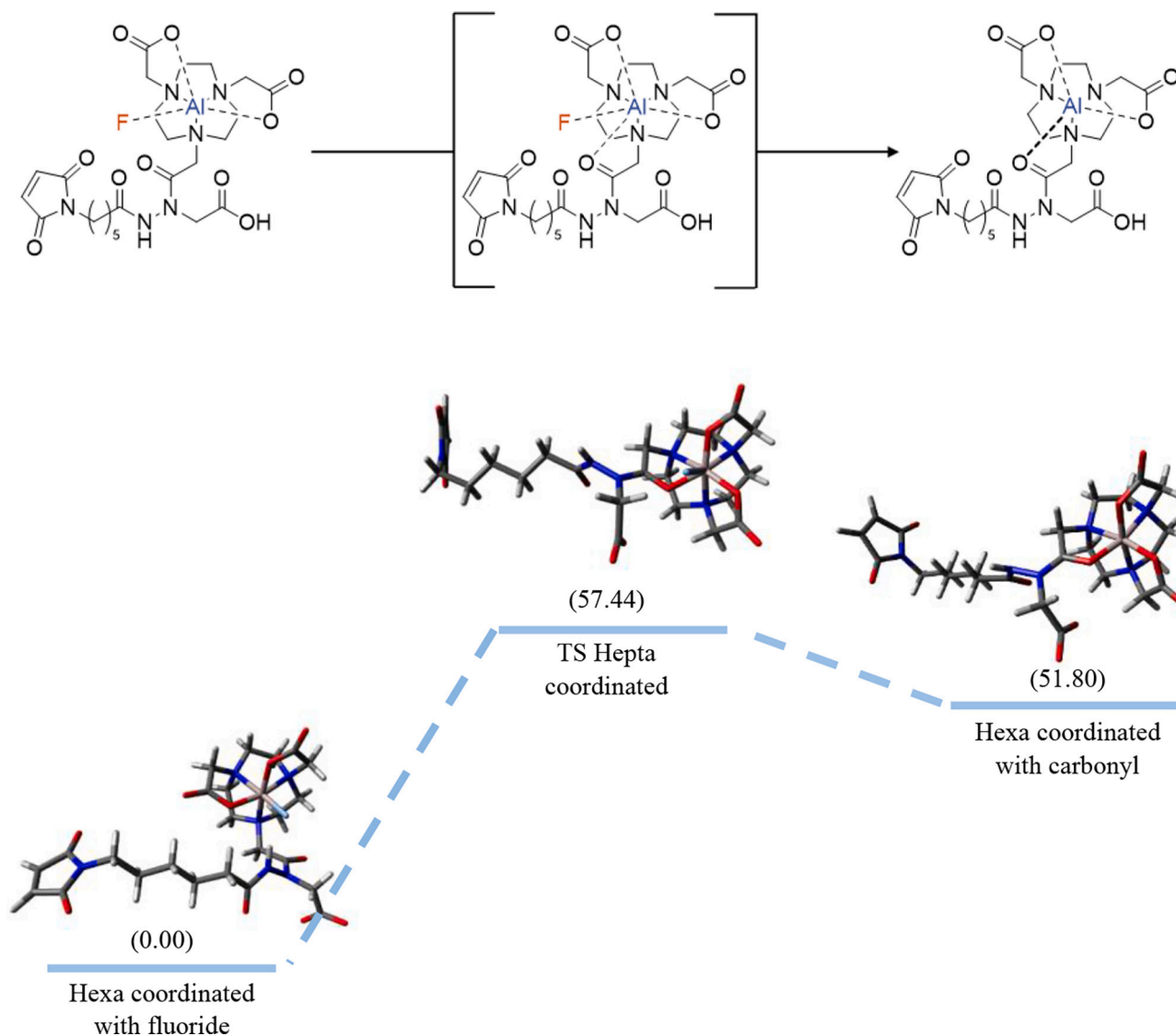


Fig. 5. Evaluation of defluorination reaction from AlF-NO2A-AHM to Al-NO2A-AHM conformation (free energy values in kcal.mol⁻¹).

oxygen atom of the carbonyl group). The average Lu—N and Lu—O_{carboxylic acid} coordination bond lengths of the Hepta_Lu structure were close to Lu—N and Lu—O bond lengths in Hexa_Lu_arm (Lu—N length of 2.543 Å and 2.527 Å respectively and Lu—O_{carboxylic acid} of 2.192 Å and 2.148 Å, respectively). The Lu—O_{carbonyl} coordination bond length was instead longer than Lu—O_{carboxylic acid} bonds (2.337 Å). This bond lengths demonstrated the lowest implication of the carbonyl group as donor compared to oxygen of carboxylic acid. Nevertheless, this carbonyl group was fundamental to slightly increase the stability of the complex as the free energy of Hepta_Lu was lower than the one of Hexa_Lu_arm (ΔE : 1.31 kcal.mol⁻¹) (Table SI-4).

2.2.2. Modeling of defluorination reaction

To test the stability of AIF-NO2A-AHM, defluorination was modeled exploring the free energy profile along the progressively increase of the distance between the fluoride from the aluminum starting from the Hexa_Al_F geometry (Fig. 5). A high energy barrier of 57.43 kcal.mol⁻¹ should cross to break the bond between aluminum and fluoride, confirming the strength of aluminum-fluoride complex and the robustness of the aluminum-fluoride bond. The defluorination conducted to the formation of Hexa_Al_O=C configuration, where the oxygen atom of the carbonyl function formed a coordination bond with the aluminum. This Hexa_Al_O=C geometry had a higher free energy than Hexa_Al_F (ΔG : 51.80 kcal.mol⁻¹). Thus, we may evidence that the defluorination was both kinetically and thermodynamically unfavorable. Note however that Hexa_Al_O=C had a slightly higher free energy than Hexa_Al_arm and hence should be regarded as an intermediate lately evolving to the final favorable conformation. Hexa_Al_O=C, had an octahedral geometry where aluminum was complexed by N₃O₃ donor set (complexation with the three nitrogen atoms of the NOTA cycle, the two oxygen atoms of the carboxylate group of the alkyl side chains and oxygen atom of the carbonyl group). The average Al—N and Al—O coordination bond lengths were of 2.098 and 1.862 Å and were thus similar to Al—N and Al—O bond lengths of the Hexa_Al_F geometry. The average of orthogonal angles was of 90.034° for Hexa_Al_O=C and 89.843° for Hexa_Al_F, while the average of linear angles was of 166.451° for Hexa_Al_O=C and 168.015° for Hexa_Al_F. Thus, the average of the difference between the ideal orthogonal angles (90°) and the orthogonal angles was of 6.667° and the average difference between the ideal linear angles (180°) and linear angles was of 13.549°, indicating that Hexa_Al_O=C was slightly more distorted than Hexa_Al_F which can also lead to some geometrical strains further decreasing the stability of the former.

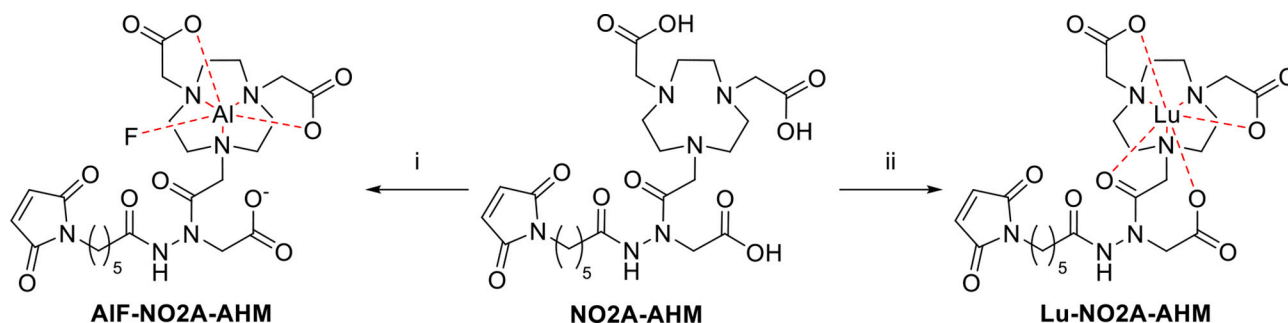
2.3. Complexation studies

Complexation evaluation was conducted using the non-radioactive mismatched pair ^{nat}F/^{nat}Lu (Scheme 2). Complexation with {Al^{nat}F}²⁺ will give a negatively charged complex, whereas Lu³⁺ will give neutral complex with NOTA as chelator.

2.3.1. Aluminum-fluoride complexation

The strategy for the complexation of NO2A-AHM with aluminum-fluoride was studied using AlCl₃ and NaF (Step (i), Scheme 2). First, {Al^{nat}F}²⁺ complex was *in-situ* synthesized by mixing 4.5 equiv. of NaF with 1.5 equiv. of AlCl₃ in 0.1 M NaOAc buffer (pH 4.5) and stirring for 5 min at RT. Then, a solution of NO2A-AHM (1 equiv.) in 0.1 M NaOAc buffer (pH 4.5) and EtOH at various ratios (Fig. 6b) was added and complexation was performed during 30 min (Scheme 2) at various temperatures (Fig. 6a). The presence of AIF-NO2A-AHM complex was confirmed by LC-MS ([M + H]⁺, *m/z* calculated 613.21, found 613.15) (Fig. SI-1). Since the optimal labeling temperature may depend on the type of chelator, the temperature impact on the conversion rate was assessed. Acyclic chelators can be complexed at low temperature (30–50 °C) such as HBED-CC [42] whereas cyclic chelators, such as NOTA, need harder temperature condition (90–110 °C). [43] For NO2A-AHM, which is a hybrid between cyclic and acyclic chelator, we tried various temperatures (40, 60, 70 and 90 °C, Fig. 6a) of complexation using a complexation media of 0.1 M NaOAc buffer (pH 4.5) with 50% EtOH. These attempts showed that the increasing temperature had a significant positive impact on the conversion rate of {Al^{nat}F}²⁺ into NO2A-AHM and a minimal temperature of 70 °C was required to reach >99% of complexation. This harsher temperature condition can be explained by the presence of the NOTA cycle. The impact of the EtOH content in the EtOH/0.1 M NaOAc buffer (pH 4.5) solvents mixture on the conversion rate was also studied (Fig. 6b) at the temperature set at 90 °C. In fact, some studies on Al¹⁸F-radiotracers demonstrated the importance of using a co-solvent such as EtOH. On one hand, D'Souza et al. suggested that a hydrophilic organic solvent would allow a better solubilization of Al¹⁸F-complex, leading to a high labeling yield. [41] On the other hand, Laverman et al. suggested that the achievement of the Al¹⁸F-reaction at lower ionic strength by adding co-solvents (e.g., EtOH, ACN) would allow a considerable increase in radiochemical conversion. [44] In our case, the conversion rate increased from 65% without EtOH to >99% with 50% EtOH (*i.e.*, EtOH/0.1 M NaOAc buffer (pH 4.5) (1/1, v/v)). Similar conclusions about EtOH impact were raised by Kang et al. for the radiolabeling of NODA chelator using aluminum-fluoride strategy. [45] In conclusion, the best conditions involving 0.1 M NaOAc buffer (pH 4.5) with 50% of EtOH at 70 °C for 30 min let to a conversion rate > 99%. AIF-NO2A-AHM complex was then directly purified by RP-HPLC to remove buffer salt and excess of NaF and AlCl₃, allowing to obtain a good yield of 75% with a high HPLC purity up to 95% under UV detection at 214 nm. No decomplexation was observed after purification using ACN and H₂O solvents containing 0.1% of TFA (pH 2).

A study concerning the formation of the {Al^{nat}F}²⁺ complex was also conducted by ¹⁹F and ²⁷Al NMR measurements. For this purpose, different solutions of AlCl₃, NaF and AlCl₃ + NaF (1 and 3 equiv. of NaF compared to AlCl₃) were prepared in D₂O or in 0.1 M NaOAc buffer (pH 4.5). Regarding the NaF samples, different ¹⁹F spectra were observed depending on whether it was solubilized in D₂O or buffer (Fig. SI-2a, yellow and green spectra). In the presence of D₂O, one singlet at -122.5



Scheme 2. AIF-NO2A-AHM and Lu-NO2A-AHM synthesis. Reagents and conditions: (i) EtOH/0.1 M NaOAc buffer at pH 4.5 (1/1, v/v), AlCl₃, NaF, 70 °C, 30 min, 75%; (ii) 0.1 M NaOAc buffer at pH 4.5, Lu(NO₃)₃, 40 °C, 30 min, 66%. The coordination bonds are represented by dotted lines.

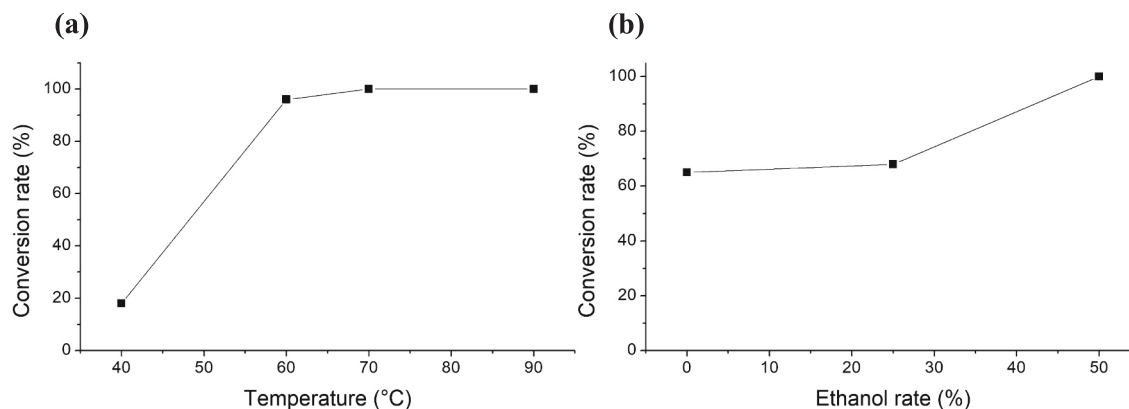


Fig. 6. (a) Influence of the temperature on the conversion rate of **AIF-NO2A-AHM**. Reaction parameters: 1.5 equiv. AlCl_3 and 4.5 equiv. NaF stirred for 5 min at RT in 0.1 M NaOAc buffer (pH 4.5) at 50% EtOH rate, then addition of **NO2A-AHM**, 30 min, 40–90 °C. (b) Influence of EtOH rate on the conversion rate of **AIF-NO2A-AHM**. Reaction parameters: 1.5 equiv. AlCl_3 and 4.5 equiv. NaF stirred for 5 min at RT in 0.1 M NaOAc buffer (pH 4.5), addition of **NO2A-AHM** and 0, 25 and 50% EtOH, 30 min, 90 °C. Conversion rate in % was measured using HPLC under a UV detection at 214 nm.

ppm was detected while the ^{19}F spectrum in the buffer presented two singlets at -121.5 and -131.0 ppm, which could be explained by some interactions between fluoride ion and NaOAc . Concerning the ^{27}Al spectrum of AlCl_3 in D_2O or in buffer (Fig. SI-2b, yellow and green spectra), according to literature data, [46] two singlets at $\delta \sim 0.6$ ppm (sharp) and at $\delta \sim 5$ ppm (broad) were observed in both solvents corresponding to hexacoordinated Al(III) ions as $[\text{Al}(\text{D}_2\text{O})_6]^{3+}$ complex and oligomers, respectively. The spectrum in D_2O also presented a singlet at $\delta 63.8$ ppm which is attributable to a tetraordinated Al(III) ion. In the mixture of AlCl_3 with 1 or 3 equiv. NaF in D_2O or in buffer (Fig. SI-2a and b, purple and red spectra), significant changes were observed in both the ^{19}F and ^{27}Al spectra compared to those of AlCl_3 and NaF alone (*i.e.*, two peaks around $\delta -156$ and 157 ppm on ^{19}F spectra and one broad singlet at $\delta \sim 1.5$ ppm on ^{27}Al spectra). These modifications suggest an interaction and bond formation between Al(III) and F^- ions.

^1H NMR spectra of **NO2A-AHM** and **AIF-NO2A-AHM** were recorded in D_2O at 330 K (Fig. 7a,b). Regarding the chelating agent (Fig. 7a), the chemical shift region of 3.21–3.46 ppm revealed the presence of five singlets corresponding to the 12 protons of the NOTA cycle (*i.e.*, six methylene groups of the NOTA backbone), the singlet at $\delta 3.93$ ppm, integrating for 6 protons, was assigned to the three methylene groups of the pending acetate arms of NOTA. After complexation with $\{\text{Al}^{\text{natF}}\}^{2+}$, the ^1H NMR spectrum in the same region showed a broad multiplet (22H, 2.76–3.86 ppm) encompassing both the methylene groups of the macrocyclic backbone and two pending acetate arms (Fig. 7). The appearance of this multiplet could be explained by the ring conformational interconversion and also by the loss of chemical equivalence of the methylene group protons in the macrocycle and on the pending acetate arms upon Al(III) ion coordination. [47] ^{27}Al NMR also prove the complexation, a new broad resonance at 40.5 ppm (Fig. 7d) appeared on the spectrum of **AIF-NO2A-AHM** complex in D_2O at 300 K corresponding to a hexacoordinated Al(III) ion. [48] ^{19}F spectrum of **AIF-NO2A-AHM** showed the conversion of fluoride on aluminum(III) ion coordinated by the ligand **NO2A-AHM**, a new signal at $\delta -176.3$ ppm (Fig. 7c) appeared compared to the spectrum of AlCl_3 with 3 equiv. NaF without ligand in buffer (Fig. SI-2a in red).

Finally, the stability of the **AIF-NO2A-AHM** complex over time (from 0 to 6 h) was studied in 0.1 M PBS (pH 7.4), H_2O , and 0.1 M NaOAc (pH 4.5) at RT by RP-HPLC analysis under UV detection at 214 nm (Fig. 8). Neither defluorination nor decomplexation of $\{\text{Al}^{\text{natF}}\}^{2+}$ were observed during this time range.

2.3.2. Lutetium complexation

For the complexation with Lu(III) , 1.5 equiv. of $\text{Lu}(\text{NO}_3)_3$ was added to **NO2A-AHM** in 0.1 M NaOAc buffer (pH 4.5) for at least 30 min

(Scheme 2). The impact of the two previously discussed factors (*i.e.*, temperature and EtOH rate) on the conversion rate was also examined (a). The results showed the success of labeling for all temperatures tested (25, 40 and 90 °C, Fig. 9a) with a kinetic complexation that increased with temperature. The presence of **Lu-NO2A-AHM** complex was confirmed by LC-MS ($[\text{M} + \text{H}]^+$, m/z calculated 741.17, found 741.15) (Fig. SI-3). In addition, evaluation of duration influence was studied and allowed to obtain a conversion rate of 94% after 3.5 h at RT compared to 60% after 30 min at RT (data not shown). Like the hybrid chelator 3p-C-NE3TA, containing both cyclic and acyclic chelator systems (one NOTA and one pendant carboxylic acid arm), [49] **NO2A-AHM** can be labeled efficiently with $^{177}\text{Lu}^{3+}$ under mild conditions. A fast kinetic complexation at a lower temperature with a high complex stability can be observed in the presence of acyclic chelator systems having enough rigidity. [50] For example, Chong et al. carried out kinetic complexation studies of $^{177}\text{Lu}^{3+}$ under mild conditions (pH 5.5, RT) for the hybrid chelators 3p-C-NETA and 3p-C-NE3TA (the only difference between the two is the presence of a second pendant carboxylic acid arm in 3p-C-NETA). [49] The results showed a much faster kinetic complexation for 3p-C-NETA with a radiolabeling efficiency of 100% in 1 min compared to 95% in 60 min for 3p-C-NE3TA. No co-solvent was necessary to complex lutetium to **NO2A-AHM** differently from the case of **AIF-NO2A-AHM**, and EtOH decreased conversion rate (Fig. 9b). In conclusion, the best conditions for lutetium complexation were 40 °C in 0.1 M NaOAc buffer (pH 4.5) for 30 min, leading to a conversion rate of 96%. **Lu-NO2A-AHM** complex was directly purified by RP-HPLC to remove buffer salt and excess of $\text{Lu}(\text{NO}_3)_3$. HPLC purification needs to be performed without 0.1% TFA in ACN and H_2O solvents, otherwise 35% decomplexation was observed after purification. We suggest that the low pH of the purification solvent (0.1% of TFA, pH 2) is the cause of this decomplexation. **Lu-NO2A-AHM** was obtained in good yield of 66% with a high HPLC purity of over 98% under UV detection at 214 nm.

Comparison of the ^1H NMR spectra of compounds **NO2A-AHM** and **Lu-NO2A-AHM** shows a change in the clumps corresponding to the ring protons (Fig. 10) and provides evidence for the complexation of Lu^{3+} by **NO2A-AHM**. After complexation with Lu^{3+} , the ^1H NMR spectrum showed an integrating bulk for twelve protons in the region of $\delta 2.90$ – 3.40 ppm containing overlapping low-resolution multiplets due to the duplication of the 12 protons of the NOTA ring (N- CH_2 - CH_2 -N ring) (initially in the region of $\delta 3.21$ – 3.46 ppm). The singlet initially observed at $\delta 3.93$ integrating for the three alkyl side chains (3 N- CH_2 - COO^-) turned into two broad singlets. These multiplets can be explained by ring conformational interconversions and protons in the alkyl side chains that are no longer equivalent upon coordination.

The complex was moderately stable in PBS with 53% of intact **Lu-**

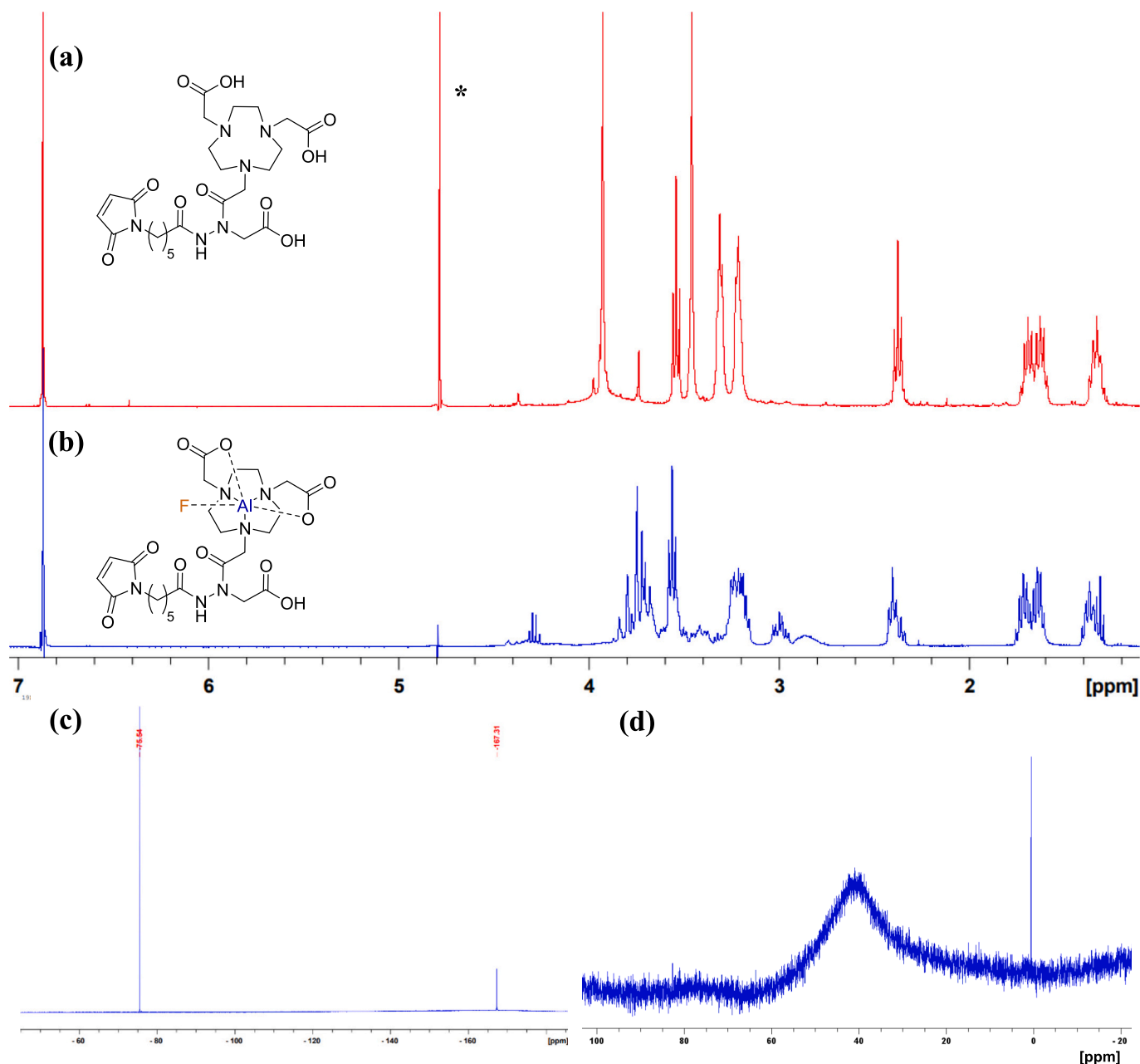


Fig. 7. ^1H NMR spectra of (a) **NO2A-AHM** and (b) **AIF-NO2A-AHM** in D_2O at 330 K (400 MHz) (peak at δ 4.75 ppm corresponds to H_2O), (c) ^{19}F NMR spectrum of **AIF-NO2A-AHM** in D_2O at 300 K (376.5 MHz) (peak at δ -75.54 ppm corresponds to TFA), (d) ^{27}Al NMR spectrum of **AIF-NO2A-AHM** in D_2O at 300 K (104.26 MHz) (*: Trace of H_2O in D_2O).

NO2A-AHM presented after 17 days. However, only 8% and 11% of decomplexation product was observed after 18 days in NaOAc buffer and water, respectively. (Fig. 11). During the stability study, only the decomplexation product (i.e., **NO2A-AHM**) was identified, and no degradation product was observed.

2.4. Radiolabeling

The ability of **NO2A-AHM** to complex non-radioactive $\{\text{Al}^{\text{nat}}\text{F}\}^{2+}$ and $^{\text{nat}}\text{Lu}^{3+}$ in a stable manner was determined by complexation and stability assays, and confirmed by molecular modeling. Thus, a proof of concept of the ability of **NO2A-AHM** to complex aluminium-fluoride-18 and lutetium-177 was conducted.

2.4.1. Radiosynthesis of $[\text{F}^{18}]\text{AIF-NO2A-AHM}$

Several protocols of $\text{Al-}^{18}\text{F}$ -radiolabeling were reported in the literature, [14,51] and different teams such as Kang et al. and Kersemans et al. demonstrated that a high ratio of co-solvent such as EtOH (60–80%) and buffer at pH around 4.5–5.0 allowed to obtain high labeling yield. [45,52] In this work, the radiolabeling strategy of **NO2A-AHM** was adapted from the reaction conditions described by Kang et al. [45]

The radiosynthesis consisted in the production of $[\text{F}^{18}]\text{NaF}$ followed by its addition to a solution of AlCl_3 (7 μg , 0.6 equiv. in a solution of 0.5 M NaOAc buffer (pH 4.5)/EtOH (20/80, v/v)) for 5 min at RT to form a $\{\text{Al}^{18}\text{F}\}^{2+}$ complex. Then, **NO2A-AHM** (30 μg , 53 nmol, 1 equiv.) was radiolabeled with $\{\text{Al}^{18}\text{F}\}^{2+}$ (50 MBq) for 15 min at 90 °C in a solution of 0.5 M NaOAc buffer (pH 4.5)/EtOH (20/80, v/v). The impact of the AlCl_3 equiv. on the conversion rate was also studied. Results presented

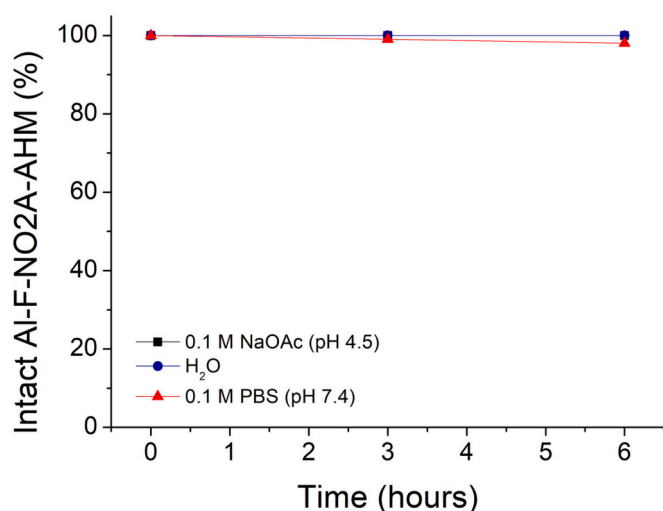


Fig. 8. RP-HPLC stability over time of the complexed AIF-NO2A-AHM (1 mg/mL) in 0.1 M NaOAc (pH 4.5), H₂O, and 0.1 M PBS (pH 7.4) at RT under UV detection (214 nm).

in Fig. SI-4a showed that 0.6 equiv. of AlCl₃ allowed to obtain the best radiochemical yield of $76 \pm 8\%$ ($n = 4$). The final pH was of 5.1 ± 0.1 ($n = 4$) and the average molar activity was $Am = 1.0 \pm 0.1$ MBq/nmol calculated as the ratio between the total activity and the molar amount of NO2A-AHM used for radiosynthesis. Evaluation of the complexation stability of the radiotracer with {Al¹⁸F}²⁺ was determined by radio-HPLC analysis for 3 h and showed no decomplexation or degradation (Fig. SI-4b).

2.4.2. Preliminary study of radiosynthesis of [¹⁷⁷Lu]Lu-NO2A-AHM

Lutetium-177 radiolabeling assays of BFC NO2A-AHM were conducted according to radiolabeling conditions used for the lutetium-177 radiolabeling of PSMA-I&T on EasyOne® (Trasis) whose protocol has been validated for clinical routine. Briefly, 380 ± 30 MBq of [¹⁷⁷Lu]LuCl₃ in 0.4 mL of 0.1 M HCl was added to a solution of NO2A-AHM (20 μg, 35 nmol) in 0.56 M NaAsc (2 mL) to reach a pH of 4.5. Radiolabeling was performed for 30 min at 90 °C. The determination of the radiochemical conversion rate was performed using radio-HPLC and radio-TLC techniques. Only 0.3% of a radiolabeled product was measured in radio-HPLC with a retention time of 5.8 min. The radio-TLC analysis using iTLC-SG as stationary phase and 0.5 M citrate buffer (pH 5) as

mobile phase has confirmed this result as the non-complexed [¹⁷⁷Lu]Lu³⁺ cation with a frontal report (fr) of 0.9 was found at 98%. We expected to obtain a compound with a fr of 0.0–0.2 using this radio-TLC conditions, as observed by the team of Eryilmaz and Kilbas for [¹⁷⁷Lu]Lu-FAPI-04 and [¹⁷⁷Lu]Lu-FAPI-46. [53] These results can be explained either by an instability of the BCF, NO2A-AHM, or by the fact that the conditions employed (*i.e.*, temperature of 90 °C) do not allow to radiolabel this new BFC.

To optimize the radiochemical conversion rate, mimetic conditions used for the complexation with native lutetium have been tested. For this purpose, the NaAsc solution was replaced by a 0.7 M NaOAc solution (pH 8). Thus, 0.2 mL of the NaOAc solution was used to buffer the lutetium-177 solution in 0.1 M HCl (380 MBq, 1 mL) to adjust the radiolabeling pH to 4.5. The radiolabeling of NO2A-AHM (20 μg, 35 nmol) was performed at 40 °C for 30 min. This time, the radio-HPLC and radio-TLC chromatograms (Fig. SI-5) showed the presence of [¹⁷⁷Lu]Lu-NO2A-AHM with a radiochemical conversion rate of 24% and 42%, respectively. The average molar activity was $Am = 10.8 \pm 2.3$ MBq/nmol calculated as the ratio between the total activity and the molar amount of NO2A-AHM used for radiosynthesis. These preliminary results are therefore promising and shown the capacity of this hybrid cyclic/acyclic chelating agent to be radiolabel by lutetium-177. Obviously, an optimization of the radiolabeling conditions will be planned in the near future to validate new radiopharmaceuticals bearing this new BFC.

3. Conclusion

The combination of a NOTA cyclic chelator and an additional chelating arm on a polyfunctionalizable hydrazine unit, allows the construction of a hybrid chelator named NO2A-AHM. This study presented the evaluation of the addition of a pendant carboxylic acid arm on the NOTA chelator to increase the stability of the complex formed with lutetium regarding its complex with NOTA and propose an innovative design for the development of a chelator for theranostic application using ¹⁸F/¹⁷⁷Lu mismatched pair. The hydrazine is the main element which allow to functionalize the three elements constituting the BFC, a NOTA macrocyclic chelator, a chelating arm and a maleimide on the extremity of an alkyl spacer for bioconjugation with cysteine containing peptides. Although the maleimide-thiol bioconjugation has a lot of advantages regarding its specificity and the use of unprotected peptide, the adduct can be prone to retro Michael reaction *in vivo*. To overcome this possibility, other bioconjugation strategies could be implemented such as the use of 3-arylpropionitriles instead of the

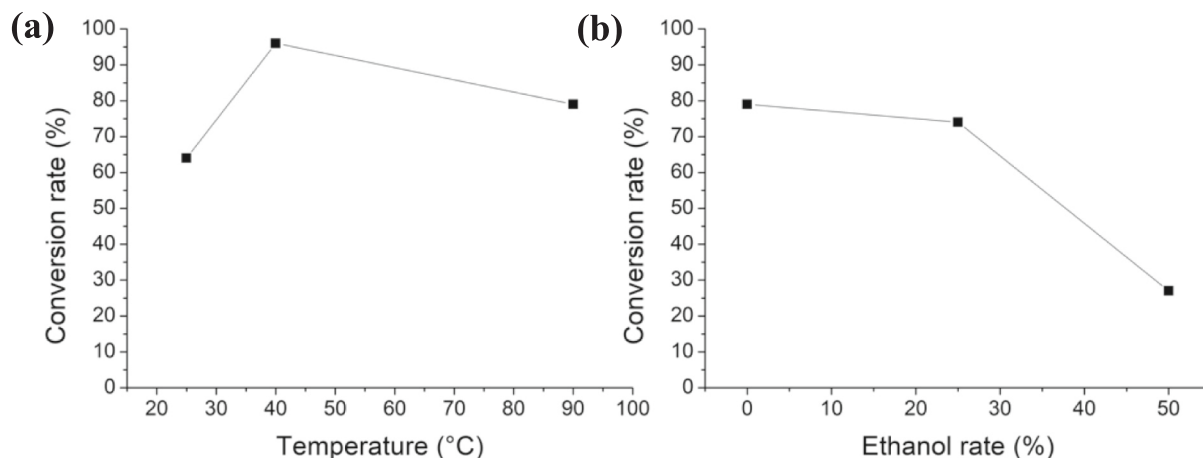


Fig. 9. (a) Influence of the temperature on the conversion rate of Lu-NO2A-AHM. Reaction parameters: 1.5 equiv. Lu(NO₃)₃ and NO2A-AHM in 0.1 M NaOAc buffer (pH 4.5), 30 min, 25–90 °C. (b) Influence of EtOH rate on the conversion rate of Lu-NO2A-AHM. Reaction parameters: 1.5 equiv. Lu(NO₃)₃ and NO2A-AHM in 0.1 M NaOAc buffer (pH 4.5)/EtOH in different ratio (v/v) 30 min, 90 °C. Conversion rate in % was measured using HPLC under a UV detection at 214 nm.

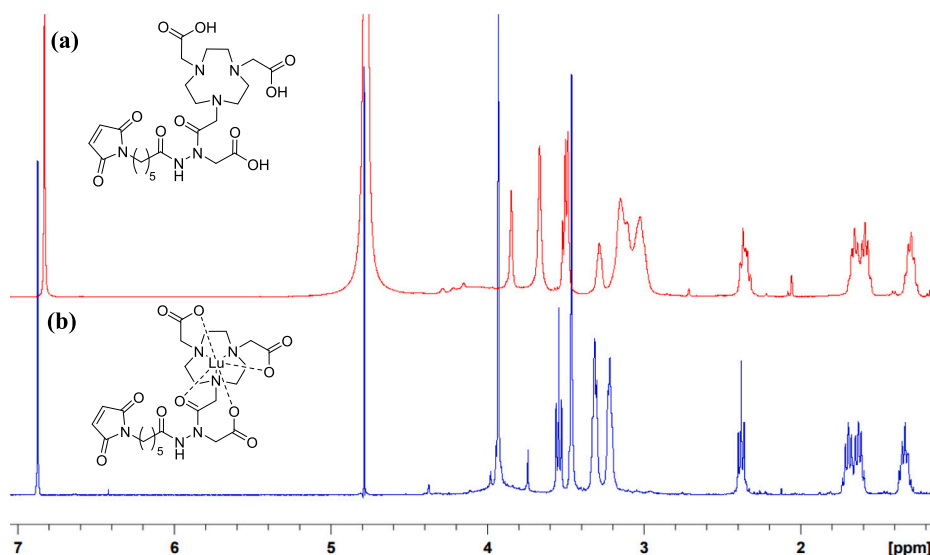


Fig. 10. ^1H NMR spectra of (a) NO2A-AHM and (b) Lu-NO2A-AHM in D_2O at 330 K (400 MHz) (peak at δ 4.75 ppm corresponds to H_2O).

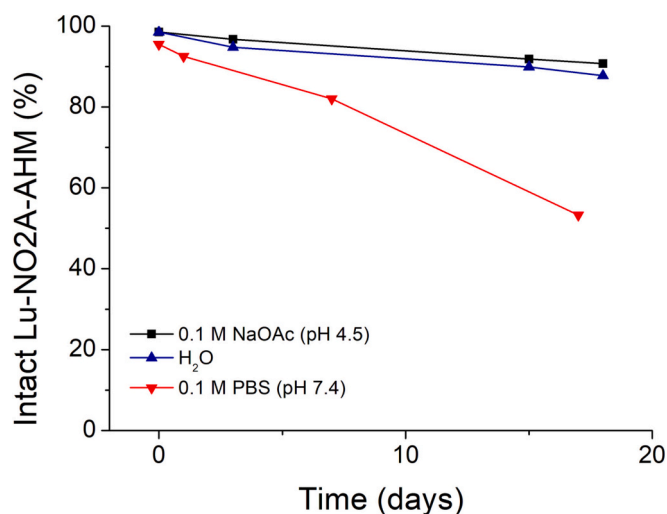


Fig. 11. RP-HPLC stability over time of the complexed Lu-NO2A-AHM (1 mg/mL) in 0.1 M NaOAc (pH 4.5), H_2O , and 0.1 M PBS (pH 7.4) at RT under UV detection (214 nm).

maleimide function, which showed selective bioconjugation with cysteine residues in the presence of other amino acid residues, and affording hydrolytically stable bioconjugates. [54] The 6 steps synthetic route explored around the polyfunctionalization of the hydrazine moiety has provided NO2A-AHM with an overall yield of 16%.

The comprehension of atoms/functions involved in the complexation around aluminum-fluoride and lutetium cations was studied by modeling calculation of the complexes. Octahedral geometries were observed for the AlF-NO2A-AHM complex and distorted pentagonal bipyramidal for Lu-NO2A-AHM. A defluorination study of the AlF-NO2A-AHM complex highlighted the very high strength of the Al-F bond and that a competition between the complexation of aluminum by the chelating arm and fluoride is not possible.

Complexation studies with the non-radioactive aluminum-fluoride $\{\text{Al}^{\text{nat}}\text{F}\}^{2+}$ and lutetium $^{\text{nat}}\text{Lu}^{3+}$ were carried out. These can be complexed by the developed BFC with conversion rates of >99% and 98%, respectively. The reference complex Al^{nat}F-NO2A-AHM has a very high stability, while the ^{nat}Lu-NO2A-AHM complex shows moderate stability after 18 days but need to be evaluated in formulated solution.

Preliminary radiolabeling tests of the new BFC with aluminum-fluoride-18 and lutetium-177 were undertaken. Thus, a radiochemical conversion rate of 76% and 24% were obtained for the compound $[\text{F}^{18}\text{AlF-NO2A-AHM}]$ and $[\text{Lu}^{177}\text{Lu-NO2A-AHM}]$, respectively.

This study demonstrates the proof of concept that this new BFC could be used to complex both aluminum-fluoride and lutetium. Further optimizations will be necessary both to increase the radiochemical conversion rate and to have stable radioconjugate in the purpose to use this new bifunctional chelator in radiopharmaceutical agents. This work is the first step in the development of theranostic agents using the mismatched pairs $^{18}\text{F}/^{177}\text{Lu}$. However, a particular attention will be given to pharmacokinetic properties evaluation. Indeed, $[\text{F}^{18}\text{AlF-NO2A-AHM}]$ is a negatively charge complex whereas $[\text{Lu}^{177}\text{Lu-NO2A-AHM}]$ is a neutral complex. The versatility of NO2A-AHM to complex other radiometal like gallium-68 and copper-64 is under investigation.

Access to radiopharmaceutical using this BFC coupled by thiol-maleimide click chemistry reaction to targeting agents containing cysteine moieties is under evaluation. Thus, radiopharmaceuticals containing cysteine amino acid and DUPA recognition pattern could be used to target PSMA receptors for prostate cancer diagnosis and treatment applications. Moreover, cysteine or thiol containing targeting agents could be evaluated to show the versatility of the BFC to be coupled to several targeting agents. The coupling of NO2A-AHM to targeting agents containing cysteine amino acid, will conduct to get access to new radiopharmaceuticals. *In vitro* and *in vivo* evaluations including stability experiments of radioconjugates could be performed to conclude about the potential of this new BFC in the development of new theranostic agents.

4. Experimental section

4.1. Reagents and general methods

All chemicals were purchased at the highest purity commercially available and were used without further purification. Dry solvents were obtained by distillation over P_2O_5 under an argon atmosphere or dried with sieves and other reagent-grade solvents were used as received. NO2AtBu was purchased from CheMatech (Dijon, France). 2-(1*H*-7-Aza-benzotriazol-1-yl)-1,1,3,3-tetramethyluronium hexafluorophosphate (HATU) was purchased from Iris Biotech GmbH (Marktredwitz, Germany). The hydrazine monohydrate, *tert*-butyl carbazate, *N*-methylmorpholine (NMM), trifluoroacetic acid (TFA), and $\text{Lu}(\text{NO}_3)_3$ were purchased from Alfa Aesar (Haverhill, MA, USA). 6-maleimido-hexanoic

acid, *tert*-butyl bromoacetate, NaF and AlCl₃ were obtained from Sigma-Aldrich (Taufkirchen, Germany). Bromoacetyl bromide and pyridine were purchased from Acros Organics. Potassium carbonate was purchased from Fluka Chemika. Chelex100® was purchased from BioRad. All products were used without further purification. Only Milli-Q water (18.2 MΩ.cm⁻¹) was used for the aqueous solutions preparation. All reactions were realized under nitrogen atmosphere.

Centrifugation was performed using Eppendorf 5810 R centrifuge. Product purifications were performed using Geduran 60H Silica Gel (63–200 mesh) flash chromatography. Preparative HPLC experiments were conducted with a Varian setup equipped with 2 Prostar 210 pumps, a reversed phase Varian Pursuit5 column (5 μm, 21.2 × 150 mm), a Prostar 335 Varian PDA UV-visible detector and a Prostar 363 Varian fluorescence detector. Data acquisition was performed by Varian Star Chromatography software. The column was used at 10 mL.min⁻¹ flow rate and the injection volume was of 10 mL. Purification was performed at 308 nm. Mobile phase A was H₂O with 0.1% of TFA and the mobile phase B was ACN with 0.1% TFA.

1D and 2D NMR spectra (¹H, ¹³C, 2D COSY, 2D HSQC, 2D HMBC) were recorded on a Bruker Advance 300 spectrometer in CDCl₃ or DMSO-*d*₆ or D₂O at 300 K on the facility of the APPEL platform of LCPM, Nancy, France expected for 1D and 2D NMR spectra (¹H, ¹³C, ¹⁹F, ²⁷Al, 2D COSY, 2D HSQC, 2D HMBC) of the compounds **NO2A-AHM**, **AIF-NO2A-AHM** and **Lu-NO2A-AHM** which were recorded on a Bruker Advance 400 spectrometer in D₂O at 300 or 330 K on the CPM NMR facility of Université de Lorraine, Nancy, France. Chemical shifts (δ) were reported in parts per million (ppm) and were referenced to the signal of CDCl₃ (δ = 7.26 and 77.16 ppm for ¹H and ¹³C NMR, respectively) or DMSO-*d*₆ (δ = 2.50 and 39.52 ppm for ¹H and ¹³C NMR, respectively) or D₂O (δ = 4.79 ppm for ¹H NMR). Coupling constants (*J*) are given in hertz (Hz) and the multiplicity is defined as *s* for singlet, *d* for doublet, *t* for triplet, *m* for multiplet, *br* for broad or combinations thereof (NMR in Fig. SI-1-11).

Analytical HPLC-MS analysis was performed on a Shimadzu LC-MS-2020, monitored by a Diode Array Detector SPD-M20A and Mass Spectroscopy Detector (Shimadzu, Marne la Vallée, France) using a Pursuit 5® C18 column (150 × 4.6 mm, 5 μm, Varian) (Varian, Agilent Technologies, Santa Clara, CA, USA). The column was used at 0.8 mL.min⁻¹ flow rate of a gradient from 5 to 100% of B (A = ACN/H₂O 5/95, 0.1% of formic acid; B = ACN, 0.1% formic acid) for 15 min. The mobile phase A was ACN/H₂O 5/95 v/v with 0.1% of formic acid and the mobile phase B was ACN with 0.1% formic acid. The flow rate was 0.8 mL.min⁻¹. The positive ions ionization ESI mode was applied (HPLC-MS in Fig. SI-1-11).

High resolution mass spectrometry (HRMS) experiments were performed on a microTOF Bruker (electrospray ionization ESI+, 50–1000 in low and 50–2500 in width).

4.2. Organic synthesis

4.2.1. Synthesis of *tert*-butyl 2-(6-(2,5-dioxo-2,5-dihydro-1H-pyrrol-1-yl)hexanoyl)hydrazine-1-carboxylate (**1**)

To a stirred solution of *tert*-butyl carbazate (500 mg, 3.78 mmol) and NMM (1.65 mL, 15.1 mmol, 4 equiv.) in anhydrous DCM (10 mL) was added at 0 °C a solution of 6-maleimidoheptanoic acid (780 mg, 3.78 mmol, 1 equiv.) in anhydrous DCM (5 mL). A solution of HATU (1.43 g, 3.78 mmol, 1 equiv.) dissolved in a minimum amount of DMF was added to the reaction mixture. The reaction mixture was slowly raised to RT and stirred for 5 h. The mixture was then washed 3 times with H₂O containing 0.1% TFA (20 mL) and the aqueous phase was extracted twice with DCM (20 mL). The organic phases were combined, dried over Na₂SO₄ and the solvent was removed under reduced pressure. The crude was purified by silica flash column chromatography (DCM/EtOH, 98/2, v/v) to give **1** as yellow oil (1.15 g, yield: 91%). Analytical HPLC R_f: 10.4 min and purity: 99% (λ_{abs} = 214 nm). ¹H NMR (CDCl₃, 300 MHz) δ 1.18–1.39 (m, 2H, CH₂-CH₂-CH₂-CONH), 1.42 (s, 9H, (CH₃)₃),

1.52–1.75 (m, 4H, CH₂-CH₂-CH₂-CH₂-CONH), 2.20 (t, 2H, *J* = 7.1 Hz, CH₂-CONH), 3.47 (t, 2H, *J* = 7.1 Hz, CH₂-N-(CO)₂), 6.66 (s, 2H, HC=CH), 6.96 (br s, 1H, NH), 8.13 (br s, 1H, NH). ¹³C NMR (CDCl₃, 75 MHz) δ 25.3 (CH₂), 26.8 (2 CH₂), 28.8 (3 CH₃), 34.4 (CH₂), 39.2 (CH₂), 82.3 (C, *t*-Bu), 134.7 (2 HC=CH), 156.3 (CO₂NH), 171.5 (2 CO), 173.0 (NH-CO-CH₂). LC-MS (ESI) calculated for C₁₅H₂₃N₃O₅Na [M + Na]⁺ *m/z* 348.15, found 348.15.

4.2.2. Synthesis of 6-(2,5-dioxo-2,5-dihydro-1H-pyrrol-1-yl)hexanehydrazide (**2**)

To a solution of compound **1** (1.08 g, 3.32 mmol, 1 equiv.) in DCM (5 mL) was added TFA (5.1 mL, 66.4 mmol, 20 equiv.) for deprotection of the Boc group. The reaction mixture was stirred at rRT for 5 h. TFA was co-evaporation four times with DCM (125 mL). The residue was precipitated in cooled Et₂O (40 mL, -20 °C). The solution was centrifugated 15 min at 5000 rpm and the supernatant was removed. The white powder was dried under vacuum (746 mg, yield: quantitative). Analytical HPLC R_f: 6.3 min and purity: 90% (λ_{abs} = 214 nm). ¹H NMR (DMSO-*d*₆, 300 MHz) δ 1.12–1.34 (m, 2H, CH₂-CH₂-CH₂-CONH), 1.39–1.61 (m, 4H, CH₂-CH₂-CH₂-CH₂-CONH), 2.16 (t, 2H, *J* = 7.3 Hz, CH₂-CO-NH), 3.38 (t, 2H, *J* = 6.9 Hz, CH₂-N-(CO)₂), 7.01 (s, 2H, HC=CH), 10.44 (s, 1H, NH). ¹³C NMR (DMSO-*d*₆, 75 MHz) δ 24.1 (CH₂), 25.5 (CH₂), 27.6 (CH₂), 32.5 (CH₂-CO), 38.7 (CH₂-N), 134.4 (2 HC=CH), 171.0 (2 CO), 171.6 (CO). LC-MS (ESI) calculated for C₁₀H₁₆N₃O₃ [M + H]⁺ *m/z* 226.11, found: 226.10.

4.2.3. Synthesis of *tert*-butyl 6-(2,5-dioxo-2,5-dihydro-1H-pyrrol-1-yl)hexanamido)glycinate (**3**)

Compound **2** (300 mg, 1.33 mmol, 1 equiv.) and K₂CO₃ (202.5 mg, 1.46 mmol, 1.1 equiv.) was dissolved in cooled DMF (15 mL, 0 °C). *Tert*-butyl bromoacetate (197 μL, 1.33 mmol, 1 equiv.) was dissolved in anhydrous DMF (5 mL) and added dropwise during 2 h to the stirred solution. The reaction mixture was slowly raised to RT and stirred overnight. Then, the reaction mixture was diluted in H₂O (100 mL) and the resulted solution was extracted thrice with EtOAc (30 mL). The organic phase was dried over Na₂SO₄ and the solvent was removed under reduced pressure. The crude was purified by silica flash column chromatography (EtOAc/*n*-hexane, 80/20, v/v) to give compound **3** as a yellow oil (238 mg, yield: 53%). Analytical HPLC R_f: 10.9 min and purity: 98% (λ_{abs} = 214 nm). ¹H NMR (CDCl₃, 300 MHz) δ 1.12–1.37 (m, 2H, CH₂-CH₂-CH₂-CONH), 1.45 (s, 9H, 3 CH₃), 1.52–1.78 (m, 4H, CH₂-CH₂-CH₂-CH₂-CONH), 2.10 (t, 2H, *J* = 7.3 Hz, CH₂-CO-NH), 3.44–3.57 (m, 4H, CH₂-N-(CO)₂, NH-CH₂-COO), 6.66 (s, 2H, HC=CH), 7.17 (br s, 1H, NH), 7.49 (br s, 1H, NH). ¹³C NMR (CDCl₃, 75 MHz) δ 25.5 (CH₂), 26.9 (CH₂), 28.8 (3CH₃), 28.8 (CH₂), 35.0 (CH₂), 38.2 (N-CH₂), 53.9 (NH-CO₂) 82.45 (C, *t*-Bu), 134.7 (2 HC=CH), 171.0 (2 CO), 171.5 (CONH), 172.6 (CONH). LC-MS (ESI) calculated for C₁₆H₂₆N₃O₅ [M + H]⁺ *m/z* 340.17, found 340.10.

4.2.4. Synthesis of *tert*-butyl *N*-(2-bromoacetyl)-*N*-(6-(2,5-dioxo-2,5-dihydro-1H-pyrrol-1-yl)hexanamido)glycinate (**4**)

To a solution of compound **3** (238 mg, 0.70 mmol, 1 equiv.) and pyridine (85 μL, 1.05 mmol, 1.5 equiv.) in anhydrous DCM (2 mL) was added dropwise a solution of bromoacetyl bromide (47 μL, 0.56 mmol, 0.8 equiv.) in anhydrous DCM (3 mL) for 10 min at RT. The reaction solution was stirred for 10 min more before evaporation of the solvent to dryness. The residue was precipitated in cooled Et₂O (40 mL, -20 °C). The solution was centrifugated 15 min at 5000 rpm and the supernatant was removed. The white powder was dried under vacuum and used in the next step without further purification (287 mg, yield: 89%). Analytical HPLC R_f: 12.4 min and purity: 96% (λ_{abs} = 214 nm). ¹H NMR (CDCl₃, 300 MHz) δ 1.27–1.38 (m, 2H, CH₂-CH₂-CH₂-CONH), 1.47 (s, 9H, 3 CH₃), 1.54–1.78 (m, 4H, CH₂-CH₂-CH₂-CH₂-CONH), 2.25 (t, 2H, *J* = 7.1 Hz, CH₂-CONH), 2.80 (s, 2H, CH₂-COOtBu), 3.52 (t, 2H, *J* = 6.9 Hz, CH₂-N-(CO)₂), 3.84 (s, 2H, CO-CH₂-Br), 6.69 (s, 2H, HC=CH), 8.07 (br s, 1H, NH). ¹³C NMR (CDCl₃, 75 MHz) δ 25.7 (CH₂), 26.9 (CH₂), 27.2

(CH₂-Br), 28.7 (3 CH₃), 28.8 (CH₂), 34.5 (CH₂), 38.1 (N-CH₂), 50.0 (NH-CH₂) 83.6 (C, tBu), 134.7 (2 HC=CH), 168.8 (CO-NH), 169.2 (2 CO), 171.5 (CO), 172.3 (CO-NH). LC-MS (ESI) calculated for C₁₈H₂₆BrN₃O₆Na [M + Na]⁺ *m/z* 482.09, found 482.00:

4.2.5. Synthesis of di-tert-butyl 2,2'-(7-(2-(1-(2-(tert-butoxy)-2-oxoethyl)-2-(6-(2,5-dioxo-2,5-dihydro-1H-pyrrol-1-yl)hexanoyl)hydrazinyl)-2-oxoethyl)-1,4,7-triazonane-1,4-diyl)diacetate (5)

To a solution of compound 4 (94 mg, 0.20 mmol, 1 equiv.) in anhydrous ACN (10 mL) was added dropwise at rRT for 2 h a solution of NO₂ArBu (72.9 mg, 0.18 mmol, 0.9 equiv.) and DIEA (71 μL, 0.40 mmol, 2 equiv.) in anhydrous ACN (5 mL). The reaction mixture was stirred at RT during 12 h and then diluted with H₂O containing 0.1% TFA (50 mL). The aqueous phase was extracted thrice with DCM (3 × 30 mL). The organic phases were combined and washed with brine (30 mL), dried over Na₂SO₄ and the solvent was removed under reduced pressure. HPLC purification was achieved using an isocratic at 50% of B during 20 min followed by gradient of 50% to 100% of B in 15 min. Compound 5 was detected by UV at 220 nm (R_f: 14.5 min) and the collected fraction was evaporated under reduced pressure and then freeze dried. Compound 5 was obtained as a white powder (49.1 mg, yield: 37%). Analytical HPLC R_f: 13.5 min and purity: 92% (λ_{abs} = 214 nm). ¹H NMR (CDCl₃, 300 MHz) δ 1.17–1.36 (m, 2H, CH₂-CH₂-CH₂-CONH), 1.45 (s, 27H, 9 CH₃), 1.54–1.73 (m, 4H, CH₂-CH₂-CH₂-CH₂-CONH), 2.29 (t, 2H, *J* = 6.9 Hz, CH₂-CO-NH), 2.84–3.37 (m, 14H, c(N-CH₂-CH₂-N-CH₂-CH₂-N-CH₂-COOtBu), N-CH₂-COOtBu), 3.45–3.58 (m, 8H, N-CH₂-CON, 2 N-CH₂-COOtBu, CH₂-N(CO)₂), 6.67 (s, 2H, HC=CH), 10.18 (br s, 1H, NH). ¹³C NMR (CDCl₃, 75 MHz) δ 25.0 (CH₂), 26.8 (2CH₂), 28.8 (9 CH₃), 34.0 (CH₂), 38.2 (CH₂-N(CO)₂), 48.5 (2 N-CH₂), 50.7 (2 N-CH₂) 51.33 (CH₂-CON), 53.0 (2 N-CH₂), 55.4 (CO-N-CH₂-COO), 56.4 (2 N-CH₂-COO), 83.0 (2 C, tBu), 83.5 (C, tBu), 134.7 (2 HC=CH), 167.4 (NH-N-CO), 169.1 (2 COO), 170.3 (2 CO), 171.6 (COO), 173.7 (CO-NH). LC-MS (ESI) calculated from C₃₆H₆₁N₆O₁₀ [M + H]⁺ *m/z* 737.44, found 737.40.

4.2.6. Synthesis of 2,2'-(7-(2-(1-(carboxymethyl)-2-(6-(2,5-dioxo-2,5-dihydro-1H-pyrrol-1-yl)hexanoyl)hydrazinyl)-2-oxoethyl)-1,4,7-triazonane-1,4-diyl)diacetic acid (NO₂A-AHM)

To a solution of compound 5 (45.2 mg, 0.06 mmol, 1 equiv.) in DCM (2 mL) was added TFA (1.2 mL, 15.9 mmol, 260 equiv.) for tBu esters deprotection. The reaction mixture was stirred at room temperature for 5 h and then TFA was removed under reduced pressure. The residue was precipitated in cooled Et₂O (40 mL, -20 °C). The solution was centrifuged 15 min at 5000 rpm and the supernatant was removed. The white powder was dried under vacuum. HPLC purification was achieved using a gradient of 5% to 70% of B in 40 min. NO₂A-AHM was detected by UV at 308 nm (R_f: 20.9 min) and the collected fraction was evaporated under reduced pressure and then freeze dried. NO₂A-AHM was obtained as white powder (34.8 mg, yield: quantitative). Analytical HPLC R_f: 7.2 min and purity: 98% (λ_{abs} = 214 nm). ¹H NMR (D₂O, 400 MHz, 330 K) δ 1.25–1.40 (m, 2H, CH₂-CH₂-CH₂-CONH), 1.56–1.75 (m, 4H, CH₂-CH₂-CH₂-CH₂-CONH), 2.37 (t, 2H, *J* = 7.3 Hz, CH₂-CO-NH), 3.21 (s, 2H, CH₂), 3.23 (s, 2H, CH₂), 3.29 (s, 2H, CH₂), 3.31 (s, 2H, CH₂), 3.46 (s, 4H, 2 CH₂), 3.54 (t, 2H, CH₂-N(CO)₂), 3.93 (m, 8H, 3 CH₂-COOH, N-CH₂-CO-N), 6.87 (s, 2H, HC=CH). ¹³C NMR (DMSO-*d*₆, 75 MHz) δ 24.0 (CH₂), 25.7 (CH₂), 27.6 (CH₂), 32.5 (CH₂), 36.9 (CH₂-N(CO)₂), 48.9 (2 N-CH₂), 49.1 (2 N-CH₂), 49.4 (2 N-CH₂), 53.5 (CH₂-CO-N), 54.4 (3 N-CH₂-COO), 134.4 (2 HC=CH), 169.5 (NH-N-CO), 170.9 (2 CO), 171.1 (3 COOH), 171.7 (CO-NH). HRMS (ESI) calculated from C₂₄H₃₇N₆O₁₀ [M + H]⁺ *m/z* 569.2571, found 569.2549.

4.3. Complexations

4.3.1. Synthesis of AIF-NO₂A-AHM

To a AlCl₃ solution in 0.1 M NaOAc buffer at pH 4.5 (2.5 mL, 10.6 mM, 1.5 equiv.) was added NaF solution in 0.1 M NaOAc buffer at pH 4.5 (2.5 mL, 31.7 mM, 4.5 equiv.) and stirred for 5 min at RT. NO₂A-AHM

solution (1 mL, 17.6 mM, 1 equiv.) in 0.1 M NaOAc buffer (pH 4.5) and EtOH (6 mL) were added to the {Al^{III}F⁻}²⁺ solution to reach a 50% of EtOH rate into final solution. The resulted mixture solution was heated for 30 min at 90 °C. HPLC purification was achieved using a gradient of 5% to 45% of B in 30 min. AIF-NO₂A-AHM was detected by UV at 220 nm (R_f: 15.2 min) and the collected fraction was evaporated under reduced pressure and then freeze dried. AIF-NO₂A-AHM was obtained as a white powder (8.08 mg, yield: 75%). Analytical HPLC R_f: 8.4 min (C18, 10–40%B in 15 min) and purity: 96% (λ_{abs} = 214 nm). ¹H NMR (D₂O, 400 MHz, 300 K) δ 1.27–1.43 (m, 2H, CH₂-CH₂-CH₂-CONH), 1.56–1.77 (m, 4H, CH₂-CH₂-CH₂-CH₂-CONH), 2.40 (t, 2H, *J* = 7.3 Hz, CH₂-CO-NH), 2.76–4.37 (m, 22H, 11 CH₂), 6.87 (s, 2H, HC=CH). ¹³C NMR (D₂O, 100.6 MHz, 300 K) δ 24.3 (CH₂-CH₂-CH₂-CH₂-CONH), 25.5 (CH₂-CH₂-CH₂-CH₂-CONH), 27.3 (CH₂-CH₂-CH₂-CH₂-CONH), 33.1 (CH₂-CH₂-CH₂-CH₂-CONH), 37.4 (CH₂-N(CO)₂), 49.1 (N-CH₂), 49.8 (N-CH₂), 51.7 (N-CH₂), 52.8 (N-CH₂), 52.9 (N-CH₂), 53.5 (N-CH₂), 54.0 (CH₂-CO-N), 55.4 (N-CH₂-COO), 62.9 (N-CH₂-COO), 63.0 (N-CH₂-COO), 134.3 (2 HC=CH), 170.9 (NH-N-CO), 171.5 (2 CO), 173.4 (CO-NH), 176.1 (COO), 176.4 (2 COO). ¹⁹F NMR (D₂O, 376.5 MHz, 300 K) δ -176.31 ppm. ²⁷Al NMR (D₂O, 104.26 MHz, 300 K) δ 69.72 ppm. LC-MS (ESI) calculated from C₂₄H₃₅AlFN₆O₁₀ [M + H]⁺ *m/z* 613.22, found 613.15.

4.3.2. Synthesis of Lu-NO₂A-AHM

To a solution of NO₂A-AHM in 0.1 M NaOAc buffer at pH 4.5 (2 mL, 10.63 mM, 1 equiv.) was added a solution of Lu(NO₃)₃ in 0.1 M NaOAc buffer at pH 4.5 (2.5 mL, 11.42 mM, 1.5 equiv.) at RT. The solution mixture was heated for 30 min at 40 °C. HPLC purification was achieved using a gradient of 5% to 35% of B in 35 min. Lu-NO₂A-AHM was detected by UV at 214 nm (R_f: 19.4 min) and the collected fraction was evaporated under reduced pressure and then freeze dried. Lu-NO₂A-AHM was obtained as a white powder (11.16 mg, yield: 66%). Analytical HPLC R_f: 7.08 min (C18 10–50%B in 15 min) and purity: 98% (λ_{abs} = 214 nm). ¹H NMR (D₂O, 400 MHz, 300 K) δ 1.22–1.40 (m, 2H, CH₂-CH₂-CH₂-CONH), 1.49–1.77 (m, 4H, CH₂-CH₂-CH₂-CH₂-CONH), 2.25–2.46 (m, 2H, CH₂-CO-NH), 2.86–3.40 (m, 12H, 6 CH₂ (NOTA)), 3.39–3.91 (m, 10H, 3 N-CH₂-COO, CO-CH₂-N, CH₂-N(CO)₂), 6.83 (s, 2H, HC=CH). ¹³C NMR (D₂O, 100 MHz, 300 K) δ 24.2 (CH₂-CH₂-CH₂-CH₂-CONH), 25.6 (CH₂-CH₂-CH₂-CH₂-CONH), 27.4 (CH₂-CH₂-CH₂-CH₂-CONH), 33.1 (CH₂-CH₂-CH₂-CH₂-CONH), 37.5 (CH₂-N(CO)₂), 49.0 (N-CH₂), 50.3 (N-CH₂), 51.0 (N-CH₂), 51.8 (N-CH₂), 52.8 (N-CH₂), 54.5 (N-CH₂), 54.8 (CH₂-CO-N), 58.2 (N-CH₂-COO), 61.7 (N-CH₂-COO), 64.9 (N-CH₂-COO), 134.4 (2 HC=CH), 172.3 (NH-N-CO), 173.5 (2 CO), 175.6 (CO-NH), 179.4 (COO), 180.1 (2 COO). LC-MS (ESI) calculated from C₂₄H₃₄LuN₆O₁₀ [M + H]⁺ *m/z* 741.17, found 741.15.

4.4. Molecular modeling

Initial structures were generated using Avogadro 1.2.0 software [55,56] and used as input for further geometry optimization. The geometry optimization has been performed with DFT using B3LYP functionals. The 6-31G basis set was used for AIF-NO₂A-AHM study whereas basis set def2-TZVP+SDD was used for Lu-NO₂A-AHM. All the calculations have been performed using the Gaussian16 software. [57] Optimization were performed in aqueous solution with water modeled as a polarizable continuum model (PCM). Vibrational frequencies have been calculated to confirm that all the structures are local minima on the potential energy surface. Furthermore, free energy has been estimated using the rigid rotor approach. Interconversion between different conformations, and defluorination have been studied considering relaxed scans along the respective relevant coordinates using the same level of theory as for the geometries optimization.

4.5. Radiolabeling

Sodium chloride solution for injection, 0.9% (wt/v) was purchased

from B. Braun (Saint-Cloud, France). Anhydrous AlCl_3 (99.999%, trace metals basis) and NaOAc (99.99% trace metals basis) were purchased from Sigma Aldrich (Taufkircher, Germany). Acetic acid glacial (>99.85%) was supplied by Merck (Darmstadt, Germany). Anhydrous absolute EtOH was purchased from Carlo Erba (Val-de-Reuil, France). Milli-Q water ($18.2 \text{ M}\Omega\cdot\text{cm}^{-1}$) was used for the aqueous solutions preparation.

Buffer was prepared and controlled with Mettler Toledo pH-meter with InLab Micro pH electrode. Sep-Pak Accell Plus QMA Plus Light Cartridge (130 mg Sorbent per Cartridge, 37–55 μm) was purchased from Waters.

No-carrier-added fluoride-18 was produced via the ^{18}O (p,n) ^{18}F nuclear reaction on a PET Trace cyclotron (GE). The bombardment was performed at 10 μA during 5 min to provide 3.7 GBq of fluoride-18 delivered as a solution in ^{18}O -enriched water (1.6 mL). Radiolabeling steps was thanks to ThermoMixer® from Eppendorf for heating and stirring. Radiolabeling tests were performed using EasyOne® (Trasis, Ans, Belgium) for automated ^{177}Lu -complexation experiment or manually after [^{18}F]NaF production using AllInOne® synthesis module (Trasis, Ans, Belgium).

Radiosynthesis were monitored either by thin-layer chromatography (TLC). TLC plates were revealed using TLC-scanner mini-GITA® (Elysia Raytest, Straubenhardt, Germany) and by HPLC using Waters system (2695eb pump, auto sampler injector, 2998 PDA detector, NaI detector from Berthold (Bad Wildbad, Germany) controlled by Empower Software (Orlando, FL, USA). The system was equipped with an ACE® Avantor RP-C18 column (150 \times 3.0 mm, 3 μm). The mobile phase A was H_2O with 0.1% of TFA and the mobile phase B was ACN with 0.1% TFA. The peaks were detected with UV detection at 214 nm and with activity detector. This work was performed on a platform member of France Life Imaging network (grant ANR-11-INBS-0006).

4.5.1. Radiosynthesis of [^{18}F]AIF-NO2A-AHM

[^{18}F]NaF was synthesized on AllInOne® module following the protocol of Collet et al. [58] Briefly, [^{18}F]NaF was eluted from a QMA chloride cartridge with 3 mL of NaCl 0.9% with a decay-corrected (dc.) radiochemical yield (RCY) of $81 \pm 3\%$ ($n = 12$). Aluminum chloride solution at 2 mM in NaCl 0.9% (16 μL , 0.6 equiv.) and 500 μL of [^{18}F]NaF solution (50 MBq) were stirred together in 1250 μL of AcONa buffer 0.1 M pH 4.5/EtOH (20/80, v/v) at RT for 5 min. A solution of NO2A-AHM of 1 $\text{mg}\cdot\text{mL}^{-1}$ in MilliQ water was added (30 μL , 1 equiv.) and the radiolabeling was performed at 90 $^\circ\text{C}$ for 15 min using a Thermomixer (300 rpm). The radiolabeling was controlled by HPLC using a gradient of 5% to 40% of B in 15 min (flow rate of 0.6 $\text{mL}\cdot\text{min}^{-1}$) (R_t : 6.1 min) and by radio-TLC using silica plate as stationary phase and $\text{H}_2\text{O}/\text{ACN}$ (4/6, v/v) as mobile phase (fr: 0.7).

4.5.2. Radiosynthesis of [^{177}Lu]Lu-NO2A-AHM

Radiosynthesis were performed on a EasyOne® (Trasis) module. The lutetium-177 solution ($380 \pm 30 \text{ MBq}$ of [^{177}Lu]Lu $^{3+}$ in HCl 0.1 M (0,4 mL)) provided by ITM (Munich, Germany) was transferred in the reactor. The precursor solution containing NO2A-AHM solution at 1 mg/mL (20 μL) and NaAsc (0,56 M in H_2O) or NaOAc (0.14 M in H_2O) in position 3 was transferred to vial which has contained the lutetium-177 solution and then, was transferred into the reactor. The radiolabeling was performed 30 min at 40 or 90 $^\circ\text{C}$ in a sealed reactor. The reaction mixture was transferred to the final vial in position 6 to evaluate the radiolabeling efficiency and diluted with NaCl 0,9% to reach a final volume of 10 mL. The radiolabeling was controlled by HPLC using a gradient of 5% to 50% of B in 10 min (flow rate of 0.8 $\text{mL}\cdot\text{min}^{-1}$) (R_t : 5.8 min) and by radio-TLC using iTLC-SG as stationary phase and citrate buffer 0.5 M pH 5.0 as mobile phase (fr: 0.3).

CRedit authorship contribution statement

Wagner Laurène: Investigation, Validation, Writing – original draft.

Losantos Raúl: Investigation, Validation. Selmeczi Katalin: Investigation, Validation. Frochot Céline: Supervision. Karcher Gilles: Funding acquisition, Resources. Monari Antonio: Investigation, Writing – original draft. Collet Charlotte: Conceptualization, Methodology, Supervision, Project administration, Writing – original draft, Writing – review & editing. Acherar Samir: Conceptualization, Supervision, Methodology, Project administration, Writing – original draft, Writing – review & editing, Funding acquisition.

Declaration of Competing Interest

The authors declare that they have no known competing financial interests or personal relationships that could have appeared to influence the work reported in this paper.

Data availability

No data was used for the research described in the article.

Acknowledgments

We acknowledge CPM NMR facility of Université de Lorraine and the APPEL platform of LCPM for the NMR analyses. We thank N. Vêran from Nancy Hospital for assistance in lutetium radiochemistry. This work was supported by the “Ministère de l’Enseignement Supérieur, de la Recherche et de l’Innovation” (MSERI) and Nancyclotep with a Doctoral fellowship for Laurène Wagner. Raúl Losantos thanks the Universidad de La Rioja and Ministerio de Universidades for his Margarita Salas grant. Equipment used for radiolabeling essays were co-funded by the French State-Region contract CPER 2015-2020 (Contrat de Plan Etat Région-IT2MP Innovations Technologiques, Modélisation et Médecine Personnalisée), by the French Grand Est Region (IRMGE project) and by the European Union through the European Regional Development Fund “FEDER-FSE Lorraine et Massif des Vosges 2014-2020”.

Appendix A. Supplementary data

Supplementary data to this article can be found online at <https://doi.org/10.1016/j.jinorgbio.2023.112267>.

References

- [1] W.A. Weber, J. Czernin, C.J. Anderson, R.D. Badawi, H. Barthel, F. Bengel, L. Bodei, I. Buvat, M. DiCarli, M.M. Graham, J. Grimm, K. Herrmann, L. Kostakoglu, J.S. Lewis, D.A. Mankoff, T.E. Peterson, H. Schelbert, H. Schöder, B. A. Siegel, H.W. Strauss, The future of nuclear medicine, molecular imaging, and theranostics, *J. Nucl. Med. Off. Publ. Soc. Nucl. Med.* 61 (2020) 263S–272S, <https://doi.org/10.2967/jnumed.120.254532>.
- [2] L. Filippi, A. Chiaravallotti, O. Schillaci, R. Cianni, O. Bagni, Theranostic approaches in nuclear medicine: current status and future prospects, *Expert Rev. Med. Devices* 17 (2020) 331–343, <https://doi.org/10.1080/17434440.2020.1741348>.
- [3] O. Keinänen, K. Fung, J.M. Brennan, N. Zia, M. Harris, E. van Dam, C. Biggin, A. Hedt, J. Stoner, P.S. Donnelly, J.S. Lewis, B.M. Zeglis, Harnessing $^{64}\text{Cu}/^{67}\text{Cu}$ for a theranostic approach to pretargeted radioimmunotherapy, *Proc. Natl. Acad. Sci.* 117 (2020) 28316–28327, <https://doi.org/10.1073/pnas.2009960117>.
- [4] C. Müller, M. Bunka, S. Haller, U. Köster, V. Groehn, P. Bernhardt, N. van der Meulen, A. Türlér, R. Schibli, Promising prospects for $^{44}\text{Sc}/^{47}\text{Sc}$ -based Theragnostics: application of ^{47}Sc for radionuclide tumor therapy in mice, *J. Nucl. Med.* 55 (2014) 1658–1664, <https://doi.org/10.2967/jnumed.114.141614>.
- [5] C. Müller, K. Zhernosekov, U. Köster, K. Johnston, H. Dorrer, A. Hohn, N.T. van der Walt, A. Türlér, R. Schibli, A unique matched quadruplet of terbium radioisotopes for PET and SPECT and for α - and β -radionuclide therapy: an in vivo proof-of-concept study with a new receptor-targeted folate derivative, *J. Nucl. Med.* 53 (2012) 1951–1959, <https://doi.org/10.2967/jnumed.112.107540>.
- [6] S.M. Qaim, B. Scholten, B. Neumaier, New developments in the production of theranostic pairs of radionuclides, *J. Radioanal. Nucl. Chem.* 318 (2018) 1493–1509, <https://doi.org/10.1007/s10967-018-6238-x>.
- [7] R. Mansi, M. Fani, Design and development of the theranostic pair ^{177}Lu -OPS201/ ^{68}Ga -OPS202 for targeting somatostatin receptor expressing tumors, *J. Label. Compd. Radiopharm.* 62 (2019) 635–645, <https://doi.org/10.1002/jlcr.3755>.
- [8] C.A. Umbrecht, M. Benešová, R.M. Schmid, A. Türlér, R. Schibli, N.P. van der Meulen, C. Müller, ^{44}Sc -PSMA-617 for radiotheragnostics in tandem with ^{177}Lu -

- PSMA-617—preclinical investigations in comparison with 68Ga-PSMA-11 and 68Ga-PSMA-617, *EJNMMI Res.* 7 (2017) 9, <https://doi.org/10.1186/s13550-017-0257-4>.
- [9] H. Chen, O. Jacobson, G. Niu, I.D. Weiss, D.O. Kiesewetter, Y. Liu, Y. Ma, H. Wu, X. Chen, Novel “add-on” molecule based on Evans blue confers superior pharmacokinetics and transforms drugs to theranostic agents, *J. Nucl. Med.* 58 (2017) 590–597, <https://doi.org/10.2967/jnumed.116.182097>.
- [10] J.R. Ballinger, Theranostic radiopharmaceuticals: established agents in current use, *Br. J. Radiol.* 91 (2018) 20170969, <https://doi.org/10.1259/bjr.20170969>.
- [11] W.J. McBride, R.M. Sharkey, H. Karacay, C.A. D'Souza, E.A. Rossi, P. Laverman, C.-H. Chang, O.C. Boerman, D.M. Goldenberg, A novel method of 18F radiolabeling for PET, *J. Nucl. Med.* 50 (2009) 991–998, <https://doi.org/10.2967/jnumed.108.060418>.
- [12] E.W. Price, C. Orvig, Matching chelators to radiometals for radiopharmaceuticals, *Chem. Soc. Rev.* 43 (2013) 260–290, <https://doi.org/10.1039/c3cs60304k>.
- [13] H.H. Coenen, J. Ermert, 18F-labelling innovations and their potential for clinical application, *Clin. Transl. Imaging* 6 (2018) 169–193, <https://doi.org/10.1007/s40336-018-0280-0>.
- [14] S. Schmitt, E. Moreau, Radiochemistry with {Al18F}2+: current status and optimization perspectives for efficient radiofluorination by complexation, *Coord. Chem. Rev.* 480 (2023), 215028, <https://doi.org/10.1016/j.ccr.2023.215028>.
- [15] K.R. Scroggie, M.V. Perkins, J.M. Chalker, Reaction of [18F]fluoride at heteroatoms and metals for imaging of peptides and proteins by positron emission tomography, *Front. Chem.* 9 (2021), <https://doi.org/10.3389/fchem.2021.687678> (accessed March 29, 2023).
- [16] S. Banerjee, M.R.A. Pillai, F.F. Russ Knapp, Lutetium-177 therapeutic radiopharmaceuticals: linking chemistry, radiochemistry, and practical applications, *Chem. Rev.* 115 (2015) 2934–2974, <https://doi.org/10.1021/cr500171e>.
- [17] B. Mitran, S.S. Rinne, M.W. Konijnenberg, T. Maina, B.A. Nock, M. Altai, A. Vorobyeva, M. Larhed, V. Tolmachev, M. de Jong, U. Rosenström, A. Orlova, Trastuzumab cotreatment improves survival of mice with PC-3 prostate cancer xenografts treated with the GRPR antagonist 177Lu-DOTAGA-PEG2-RM26, *Int. J. Cancer* 145 (2019) 3347–3358, <https://doi.org/10.1002/ijc.32401>.
- [18] U. Pandey, N. Gamre, S.P. Lohar, A. Dash, A systematic study on the utility of CHX-A-DTPA-NCS and NOTA-NCS as bifunctional chelators for 177Lu radiopharmaceuticals, *Appl. Radiat. Isot.* 127 (2017) 1–6, <https://doi.org/10.1016/j.apradiso.2017.04.028>.
- [19] Z. Novy, A. Laznickova, J. Mandikova, P. Barta, M. Laznickek, F. Trejtnar, The effect of chelator type on in vitro receptor binding and stability in 177Lu-labeled cetuximab and panitumumab, *J. Label. Compd. Radiopharm.* 57 (2014) 448–452, <https://doi.org/10.1002/jlcr.3204>.
- [20] M.L. Lepage, H.-T. Kuo, A. Roxin, S. Huh, Z. Zhang, R. Kandasamy, H. Merckens, J. O. Kumlin, A. Limoges, S.K. Zeisler, K.-S. Lin, F. Bénard, D.M. Perrin, toward 18F-labeled Theranostics: a single agent that can be labeled with 18F, 64Cu, or 177Lu, *ChemBioChem.* 21 (2020) 943–947, <https://doi.org/10.1002/cbic.201900632>.
- [21] H. Chong, K. Garmestani, D. Ma, D.E. Milenic, T. Overstreet, M.W. Brechbiel, Synthesis and biological evaluation of novel macrocyclic ligands with pendent donor groups as potential yttrium chelators for Radioimmunotherapy with improved complex formation kinetics, *J. Med. Chem.* 45 (2002) 3458–3464, <https://doi.org/10.1021/jm0200759>.
- [22] H.-S. Chong, X. Sun, P. Dong, C.S. Kang, Convenient synthesis and evaluation of a Heptadentate bifunctional ligand for Radioimmunotherapy applications, *Eur. J. Org. Chem.* 2011 (2011) 6641–6648, <https://doi.org/10.1002/ejoc.201101063>.
- [23] H.-S. Chong, H.A. Song, X. Ma, D.E. Milenic, E.D. Brady, S. Lim, H. Lee, K. Baidoo, D. Cheng, M.W. Brechbiel, Novel bimodal bifunctional ligands for Radioimmunotherapy and targeted MRI, *Bioconjug. Chem.* 19 (2008) 1439–1447, <https://doi.org/10.1021/bc800050x>.
- [24] C.S. Kang, X. Sun, F. Jia, H.A. Song, Y. Chen, M. Lewis, H.-S. Chong, Synthesis and preclinical evaluation of bifunctional ligands for improved chelation chemistry of 90Y and 177Lu for targeted Radioimmunotherapy, *Bioconjug. Chem.* 23 (2012) 1775–1782, <https://doi.org/10.1021/bc200696b>.
- [25] C.S. Kang, H.A. Song, D.E. Milenic, K.E. Baidoo, M.W. Brechbiel, H.-S. Chong, Preclinical evaluation of NETA-based bifunctional ligand for Radioimmunotherapy applications using 212Bi and 213Bi: radiolabeling, serum stability, and biodistribution and tumor uptake studies, *Nucl. Med. Biol.* 40 (2013) 600–605, <https://doi.org/10.1016/j.nucmedbio.2013.01.012>.
- [26] S. Ahenkorah, E. Murce, C. Cawthorne, J.P. Ketcheman, C.M. Deroose, T. Cardinaels, Y. Seimbille, H. Fonge, W. Gsell, G. Bormans, M. Ooms, F. Cleeren, 3p-C-NETA: a versatile and effective chelator for development of Al^{18F}-labeled and therapeutic radiopharmaceuticals, *Theranostics.* 12 (2022) 5971–5985, <https://doi.org/10.7150/thno.75336>.
- [27] C.J. Anderson, T.J. Wadas, E.H. Wong, G.R. Weisman, Cross-bridged macrocyclic chelators for stable complexation of copper radionuclides for PET imaging, *Q. J. Nucl. Med. Mol. Imaging Off. Publ. Ital. Assoc. Nucl. Med. AIMN Int. Assoc. Radiopharmacol. IAR Sect. Soc. Of.* 52 (2008) 185–192.
- [28] J.H. Dam, B.B. Olsen, C. Baum, P.-F. Høilund-Carlson, H. Thisgaard, In vivo evaluation of a Bombesin analogue labeled with Ga-68 and co-55/57, *Mol. Imaging Biol.* 18 (2016) 368–376, <https://doi.org/10.1007/s1307-015-0911-z>.
- [29] R.P.J. Schroeder, C. Müller, S. Reneman, M.L. Melis, W.A.P. Breeman, E. de Blois, C.H. Bangma, E.P. Krenning, W.M. van Weerden, M. de Jong, A standardised study to compare prostate cancer targeting efficacy of five radiolabelled bombesin analogues, *Eur. J. Nucl. Med. Mol. Imaging* 37 (2010) 1386–1396, <https://doi.org/10.1007/s00259-010-1388-2>.
- [30] C. Baum, B. Mitran, S.S. Rinne, J.H. Dam, B.B. Olsen, V. Tolmachev, A. Orlova, H. Thisgaard, Preclinical evaluation of the Copper-64 labeled GRPR-antagonist RM26 in comparison with the Cobalt-55 labeled counterpart for PET-imaging of prostate Cancer, *Molecules.* 25 (2020) 5993, <https://doi.org/10.3390/molecules25245993>.
- [31] N. Guo, L. Lang, W. Li, D.O. Kiesewetter, H. Gao, G. Niu, Q. Xie, X. Chen, Quantitative analysis and comparison study of [18F]AlF-NOTA-PRGD2, [18F]FPFRGD2 and [68Ga]Ga-NOTA-PRGD2 using a reference tissue model, *PLoS One* 7 (2012), e37506, <https://doi.org/10.1371/journal.pone.0037506>.
- [32] R.-O. Moussodia, S. Acherar, A. Bordessa, R. Vanderesse, B. Jamart-Grégoire, An expedient and short synthesis of chiral α -hydrazinoesters: synthesis and conformational analysis of 1:1 [α -N α -Hydrazino]mers, *Tetrahedron.* 68 (2012) 4682–4692, <https://doi.org/10.1016/j.tet.2012.04.018>.
- [33] E. Romero, R.-O. Moussodia, B. Jamart-Grégoire, S. Acherar, Synthesis and conformational analysis of 1:1 [α -N α -Bn-Hydrazino] and 1:1 [α -N α -Bn-Hydrazino/ α] trimers: determination of the $\Delta\delta$ value for the γ -turn structuration, *Eur. J. Org. Chem.* 2018 (2018) 4754–4761, <https://doi.org/10.1002/ejoc.201800755>.
- [34] S.H. Bouayad-Gervais, W.D. Lubell, Examination of the potential for adaptive chirality of the nitrogen chiral center in Aza-Aspartame, *Molecules.* 18 (2013) 14739–14746, <https://doi.org/10.3390/molecules181214739>.
- [35] J. Spiegel, C. Mas-Moruno, H. Kessler, W.D. Lubell, Cyclic Aza-peptide integrin ligand synthesis and biological activity, *J. Organomet. Chem.* 77 (2012) 5271–5278, <https://doi.org/10.1016/j.jo300311q>.
- [36] A. Cheguillaume, F. Lehardy, K. Bouget, M. Baudy-Floc'h, P. Le Grel, Submonomer solution synthesis of hydrazinoazapeptides, a new class of pseudopeptides, *J. Organomet. Chem.* 64 (1999) 2924–2927, <https://doi.org/10.1021/jo9814871>.
- [37] J. Song, X. Peng, L. Li, F. Yang, X. Zhang, J. Zhang, J. Dai, M. Cui, Al18F-NODA Benzothiazole derivatives as imaging agents for cerebrovascular amyloid in cerebral amyloid Angiopathy, *ACS Omega* 3 (2018) 13089–13096, <https://doi.org/10.1021/acsomega.8b01120>.
- [38] B.E. Uno, K.K. Deibler, C. Villa, A. Raghuraman, K.A. Scheidt, Conjugate additions of amines to Maleimides via cooperative catalysis, *Adv. Synth. Catal.* 360 (2018) 1719–1725, <https://doi.org/10.1002/adsc.201800160>.
- [39] G.T. Hermanson, Chapter 3 - the reactions of bioconjugation, in: G.T. Hermanson (Ed.), *Bioconjugate Tech*, Third ed., Academic Press, Boston, 2013, pp. 229–258, <https://doi.org/10.1016/B978-0-12-382239-0.00003-0>.
- [40] S. Wang, Y. Gai, M. Li, H. Fang, G. Xiang, X. Ma, Synthesis of a new bifunctional NODA for bioconjugation with PSMA ligand and one-step Al18F labeling, *Bioorg. Med. Chem.* 60 (2022), 116687, <https://doi.org/10.1016/j.bmc.2022.116687>.
- [41] C.A. D'Souza, W.J. McBride, R.M. Sharkey, L.J. Todaro, D.M. Goldenberg, High-yielding aqueous 18F-labeling of peptides via Al18F chelation, *Bioconjug. Chem.* 22 (2011) 1793–1803, <https://doi.org/10.1021/bc200175c>.
- [42] J. Giglio, M. Zeni, E. Savio, H. Engler, Synthesis of an Al18F radiofluorinated GLU-UREA-LYS(AHX)-HBED-CC PSMA ligand in an automated synthesis platform, *EJNMMI Radiopharm. Chem.* 3 (2018) 4, <https://doi.org/10.1186/s41181-018-0039-y>.
- [43] S. Liu, H. Liu, H. Jiang, Y. Xu, H. Zhang, Z. Cheng, One-step radiosynthesis of 18F-AlF-NOTA-RGD2 for tumor angiogenesis PET imaging, *Eur. J. Nucl. Med. Mol. Imaging* 38 (2011) 1732, <https://doi.org/10.1007/s00259-011-1847-4>.
- [44] P. Laverman, C.A. D'Souza, A. Eek, W.J. McBride, R.M. Sharkey, W.J.G. Oyen, D. M. Goldenberg, O.C. Boerman, Optimized labeling of NOTA-conjugated octreotide with F-18, *Tumor Biol.* 33 (2012) 427–434, <https://doi.org/10.1007/s13277-011-0250-x>.
- [45] D. Kang, U. Simon, F.M. Mottaghy, A.T.J. Vogg, Labelling via [Al18F]2+ using Precomplexed Al-NODA moieties, *Pharmaceuticals.* 14 (2021) 818, <https://doi.org/10.3390/ph14080818>.
- [46] J.W. Akitt, Multinuclear studies of aluminium compounds, *Prog. Nucl. Magn. Reson. Spectrosc.* 21 (1989) 1–149, [https://doi.org/10.1016/0079-6565\(89\)80001-9](https://doi.org/10.1016/0079-6565(89)80001-9).
- [47] A. de Sá, M.I.M. Prata, C.F.G.C. Geraldes, J.P. André, Triaza-based amphiphilic chelators: synthetic route, in vitro characterization and in vivo studies of their Ga (III) and Al(III) chelates, *J. Inorg. Biochem.* 104 (2010) 1051–1062, <https://doi.org/10.1016/j.jinorgbio.2010.06.002>.
- [48] M. Haouas, F. Taulelle, C. Martineau, Recent advances in application of 27Al NMR spectroscopy to materials science, *Prog. Nucl. Magn. Reson. Spectrosc.* 94–95 (2016) 11–36, <https://doi.org/10.1016/j.pnmrs.2016.01.003>.
- [49] H.-S. Chong, X. Sun, Y. Chen, I. Sin, C.S. Kang, M.R. Lewis, D. Liu, V.C. Ruthengael, Y. Zhong, N. Wu, H.A. Song, Synthesis and comparative biological evaluation of bifunctional ligands for radiotherapy applications of 90Y and 177Lu, *Bioorg. Med. Chem.* 23 (2015) 1169–1178, <https://doi.org/10.1016/j.bmc.2014.12.035>.
- [50] L. Li, H.-T. Kuo, X. Wang, H. Merckens, N. Colpo, V. Radchenko, P. Schaffer, K.-S. Lin, F. Bénard, C. Orvig, t Bu4octapa-alkyl-NHS for metalloradiolabeling preparation, *Dalton Trans.* 49 (2020) 7605–7619, <https://doi.org/10.1039/D0DT00845A>.
- [51] S.J. Archibald, L. Allott, The aluminium-[18F]fluoride revolution: simple radiochemistry with a big impact for radiolabelled biomolecules, *EJNMMI Radiopharm. Chem.* 6 (2021) 30, <https://doi.org/10.1186/s41181-021-00141-0>.
- [52] K. Kersemans, K. De Man, J. Courtney, T. Van Royen, S. Piron, L. Moerman, B. Brans, F. De Vos, Automated radiosynthesis of Al[18F]PSMA-11 for large scale routine use, *Appl. Radiat. Isot. Data Instrum. Methods Use Agric. Ind. Med.* 135 (2018) 19–27, <https://doi.org/10.1016/j.apradiso.2018.01.006>.
- [53] K. Eryilmaz, B. Kilbas, Fully-automated synthesis of 177Lu labelled FAPI derivatives on the module modular lab-Eazy, *EJNMMI Radiopharm. Chem.* 6 (2021) 16, <https://doi.org/10.1186/s41181-021-00130-3>.
- [54] O. Koniev, G. Leriche, M. Nothisen, J.-S. Remy, J.-M. Strub, C. Schaeffer-Reiss, A. Van Dorsselaer, R. Baati, A. Wagner, Selective irreversible chemical tagging of

- cysteine with 3-Arylpropionitriles, *Bioconjug. Chem.* 25 (2014) 202–206, <https://doi.org/10.1021/bc400469d>.
- [55] M.D. Hanwell, D.E. Curtis, D.C. Lonie, T. Vandermeersch, E. Zurek, G.R. Hutchison, Avogadro: an advanced semantic chemical editor, visualization, and analysis platform, *J. Cheminformatics* 4 (2012) 17, <https://doi.org/10.1186/1758-2946-4-17>.
- [56] T.A. Team, Avogadro - Free Cross-Platform Molecular Editor, Avogadro. <https://avogadro.cc/>, 2023 (accessed October 26, 2022).
- [57] M.J. Frisch, G.W. Trucks, H.B. Schlegel, G.E. Scuseria, M.A. Robb, J.R. Cheeseman, G. Scalmani, V. Barone, G.A. Petersson, H. Nakatsuji, X. Li, M. Caricato, A. V. Marenich, J. Bloino, B.G. Janesko, R. Gomperts, B. Mennucci, H.P. Hratchian, J. V. Ortiz, A.F. Izmaylov, J.L. Sonnenberg, F. Ding Williams, F. Lipparini, F. Egidi, J. Goings, B. Peng, A. Petrone, T. Henderson, D. Ranasinghe, V.G. Zakrzewski, J. Gao, N. Rega, G. Zheng, W. Liang, M. Hada, M. Ehara, K. Toyota, R. Fukuda, J. Hasegawa, M. Ishida, T. Nakajima, Y. Honda, O. Kitao, H. Nakai, T. Vreven, K. Throssell, J.A. Montgomery Jr., J.E. Peralta, F. Ogliaro, M.J. Bearpark, J. J. Heyd, E.N. Brothers, K.N. Kudin, V.N. Staroverov, T.A. Keith, R. Kobayashi, J. Normand, K. Raghavachari, A.P. Rendell, J.C. Burant, S.S. Iyengar, J. Tomasi, M. Cossi, J.M. Millam, M. Klene, C. Adamo, R. Cammi, J.W. Ochterski, R.L. Martin, K. Morokuma, O. Farkas, J.B. Foresman, D.J. Fox, Gaussian, Inc., Wallingford, CT, 2016.
- [58] C. Collet, M. Otabashi, F. Giacomelli, N. Veran, G. Karcher, Y. Chapleur, S. Lamandé-Langle, Fully automated production of sodium [18F]fluoride on AllInOne and miniAllInOne synthesizers, *Appl. Radiat. Isot.* 102 (2015) 87–92, <https://doi.org/10.1016/j.apradiso.2015.04.016>.